

Double-Virtual NNLO QCD Corrections for Five-Parton Scattering: The Gluon Channel

Giuseppe De Laurentis,^{1,2} Harald Ita,^{2,3} Maximillian Klinkert,⁴ and Vasily Sotnikov⁵

¹*Higgs Centre for Theoretical Physics, University of Edinburgh, Edinburgh, EH9 3FD, United Kingdom*

²*Paul Scherrer Institut, Forschungsstrasse 111, 5232 Villigen, Switzerland*

³*ICS, University of Zurich, Winterthurerstrasse 190, Zurich, Switzerland*

⁴*Physikalisches Institut, Albert-Ludwigs-Universität Freiburg,
Hermann-Herder. Str. 3, D-79104 Freiburg, Germany*

⁵*Physik-Institut, University of Zurich, Winterthurerstrasse 190, 8057 Zurich, Switzerland*

We compute the two-loop helicity amplitudes for the scattering of five gluons, including all contributions beyond the leading-color approximation. The analytic expressions are represented as linear combinations of transcendental functions with rational coefficients, which we reconstruct from finite-field samples obtained with the numerical unitarity method. Guided by the requirement of removing unphysical singularities, we find a remarkably compact generating set of rational coefficients, which we display entirely in the manuscript. We implement our results in a public code, which provides efficient and reliable numerical evaluations for phenomenological applications.

I. INTRODUCTION

The long-term perspective of the Large Hadron Collider (LHC) at CERN serves as a compelling reason to explore new ways to advance our understanding of high-energy particle collisions beyond the level of detail and precision currently attainable.

Among the central processes under study through hadron collisions is the production of multiple jets. Notably, the recent impressive measurements of the strong coupling constant at high momentum transfer [1–3] crucially depend upon the cutting-edge next-to-next-to-leading order (NNLO) QCD predictions for three-jet production [1] (see also [4]). These predictions relied upon the leading-color approximation for double-virtual corrections [5], contributing on average about 10% [1]. This highlights the potential importance of including subleading-color effects. Moreover, the observation that the subleading-color effects can be enhanced in certain differential observables [6] underscores the necessity to study three-jet production in full color.

Looking towards the future, five-parton scattering at two loops is also a crucial ingredient in advancing towards the N³LO precision frontier for di-jet production in hadron collisions. A related intriguing application lies in the explicit examination of the breakdown of collinear factorization in QCD, which may occur at the third order in perturbation theory when subleading color effects are taken into account [7–9].

In this letter we focus on the five-gluon channel and derive compact analytic expressions for all two-loop five-gluon helicity amplitudes, including for the first time all contributions beyond the leading-color approximation. The remaining quark channels will be presented in the followup publication [10].

Five-point two-loop computations are notoriously difficult due to the unforgiving admixture of algebraic, analytic, and combinatorial complexity. This challenge is particularly pronounced when contributions from non-planar diagrams are included. Nevertheless, thanks to advancements in the understanding of the relevant Feynman integrals [11–15], and analytic reconstruction techniques [16–28], recent years have witnessed remarkable progress in computations of two-loop five-point massless amplitudes. In fact, all massless two-loop amplitudes with any combination of photons and partons in the final state are already known analytically in full color [22, 29, 30], with the exception of the five-parton process, which until now was known only in the leading-color approximation [5].

In this work we build upon this remarkable progress and, in particular, leverage the computational framework established in refs. [31–35]. We further delve into a limiting aspect of the analytic reconstruction methods in amplitude computations. Conventional approaches, in essence, employ generic rational ansätze that involve numerous unphysical singularities and redundant parameters. In stark contrast amplitudes often assume concise representations in partial fractioned form. This leads to the intriguing question: can analytic reconstruction directly yield the compact results? While we delay a more thorough discussion of this question to future work [36], we present evidence that a positive outcome can be achieved by leveraging information about the functions' singularities and residues. In fact, considering two-loop five-gluon scattering in full color, we obtain a representation that seamlessly fits into the appendix of this letter. With the exception of special helicity configurations [37–39], this level of simplicity has been notably elusive for five-point two-loop scattering.

Finally, we provide a C++ library for fast numerical evaluation of the NNLO hard function that is ready for use in cross-section computations. Together with the upcoming results for the quark channels that we will make available in the followup publication [10], these results will provide crucial input for NNLO cross-section computations.

Note added: while this work was in preparation, we became aware of ref. [40], which reports partially overlapping results. We thank the authors for the numerical comparison of our results and for coordinating the publications.

II. NOTATION AND CONVENTIONS

We consider the $\mathcal{O}(\alpha_s^2)$ corrections to the scattering of five-gluons. This requires the computation of two-loop five-gluon scattering amplitudes, which we obtain omitting the contributions from the massive top quark. Furthermore, we treat all quarks as massless states. The contributing partonic process is

$$g(-p_1^{-h_1}) + g(-p_2^{-h_2}) \rightarrow g(p_3^{h_3}) + g(p_4^{h_4}) + g(p_5^{h_5}). \quad (1)$$

Here p_i and h_i denote the momentum and the helicity of the i^{th} particle, respectively. Unless stated otherwise, throughout this paper, momenta and helicity labels are understood in the all-outgoing convention. Representative Feynman diagrams for the two-loop contributions are shown in fig. 1.

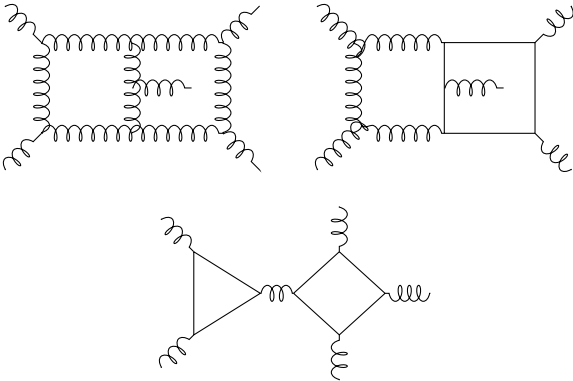


Figure 1: Representative Feynman diagrams for two-loop five-gluon amplitudes. Solid lines represent closed massless quark loops.

A. Kinematics

The process involves five massless particles. The underlying scattering kinematic can therefore be specified by five Mandelstam invariants $\{s_{12}, s_{23}, s_{34}, s_{45}, s_{15}\}$, as well as the parity-odd contraction of four momenta $\text{tr}_5 = \text{tr}(\gamma^5 \not{p}_1 \not{p}_2 \not{p}_3 \not{p}_4)$.

To represent the dependence of scattering amplitudes on the particles' helicities we use two-component spinors, λ_i^α and $\tilde{\lambda}_i^{\dot{\alpha}}$, with $i \in \{1, \dots, 5\}$. We define the invariant contractions of spinors as

$$\langle ij \rangle = \lambda_i^\alpha \lambda_{j,\alpha} \quad \text{and} \quad [ij] = \tilde{\lambda}_{i,\dot{\alpha}} \tilde{\lambda}_j^{\dot{\alpha}}, \quad (2)$$

which are related to the Mandelstam invariants through $s_{ij} = \langle ij \rangle [ji]$ (see e.g. [41] for matching conventions). We will also use longer spinor contractions, in particular

$$\langle ij \pm k | i \rangle = \langle ij \rangle [ji] \pm \langle ik \rangle [ki]. \quad (3)$$

Finally, we can express tr_5 as a polynomial in spinor brackets as¹

$$\text{tr}_5 = [12] \langle 23 \rangle [34] \langle 41 \rangle - \langle 12 \rangle [23] \langle 34 \rangle [41]. \quad (4)$$

A little-group transformation of the i^{th} leg with helicity h_i reads $(\lambda_i, \tilde{\lambda}_i) \rightarrow (z_i \lambda_i, \tilde{\lambda}_i / z_i)$. Under this transformation, the helicity amplitudes transform as $A \rightarrow z_i^{-2h_i} A$. We refer to the exponent of the z_i as the little-group weight.

B. Color space

The external gluons are in the adjoint representation of $SU(N_c)$ and carry indices $\vec{a} = \{a_1, \dots, a_5\}$ which run over $N_c^2 - 1$ values. We explicitly represent the five-gluon amplitudes in the color space through the trace basis as [42]

$$\begin{aligned} \mathcal{A}_{\vec{a}} = & \sum_{\sigma \in \mathcal{S}_5 / \mathbb{Z}_5} \sigma \left(\text{tr}(1, 2, 3, 4, 5) A_1(1, 2, 3, 4, 5) \right) + \\ & \sum_{\sigma \in \frac{\mathcal{S}_5}{\mathbb{Z}_2 \times \mathcal{S}_3}} \sigma \left(\text{tr}(1, 2) \text{tr}(3, 4, 5) A_2(1, 2; 3, 4, 5) \right), \quad (5) \end{aligned}$$

where $\text{tr}(i_1, \dots, i_n) = \text{tr}(T^{a_{i_1}} \dots T^{a_{i_n}})$, and T^{a_i} are the hermitian and traceless generators of fundamental representation of $SU(N_c)$. The permutation $\sigma = \{i_1, \dots, i_5\}$ acts on all external-particle labels as

¹ We note that tr_5 in ref. [5] differs by a minus sign compared to this definition.

$\sigma(i) = \sigma_i$. The sums run over all permutations that do not leave the respective traces invariant. Thus, the first sum runs over 24 elements, while the second one runs over 20 elements.

The generators T^a are normalized as,

$$\text{tr}(T^a T^b) = \delta^{ab}, \quad (6)$$

and fulfill the commutator relations,

$$[T^a, T^b] = if_{abc} T^c, \quad (7)$$

$$if_{abc} = \text{tr}(T^a T^b T^c) - \text{tr}(T^b T^a T^c). \quad (8)$$

The amplitudes A_i admit an expansion in terms of the bare QCD coupling constant $\alpha_s^0 = (g_s^0)^2/(4\pi)$,

$$A_i = (g_s^0)^3 \left(\sum_{L=0}^2 \left(\frac{\alpha_s^0}{2\pi} \right)^L A_i^{(L)} + \mathcal{O}((\alpha_s^0)^3) \right) \quad (9)$$

with L denoting the number of loops. In this work we consider an arbitrary number of light quark flavors in the loops that is denoted by N_f . The five-gluon amplitudes can be further expanded in powers of N_c and N_f through two loops as follows,

$$A_1^{(0)} = A^{(0),(0,0)}, \quad A_2^{(0)} = 0, \quad (10a)$$

$$A_1^{(1)} = N_c A^{(1),(1,0)} + N_f A^{(1),(0,1)}, \quad (10b)$$

$$A_2^{(1)} = A^{(1),(0,0)}, \quad (10c)$$

$$A_1^{(2)} = N_c^2 A^{(2),(2,0)} + \mathbf{A}^{(2),(0,0)} \quad (10d)$$

$$+ N_f N_c A^{(2),(1,1)} + \frac{N_f}{N_c} \mathbf{A}^{(2),(-1,1)} \\ + N_f^2 A^{(2),(0,2)},$$

$$A_2^{(2)} = N_c A^{(2),(1,0)} \quad (10e)$$

$$+ N_f \mathbf{A}^{(2),(0,1)} + \frac{N_f^2}{N_c} \mathbf{A}^{(2),(-1,2)}.$$

The coefficients $A^{(L),(n_c, n_f)}$, which we call *partial amplitudes*, are uniquely identified by the three integers L, n_c, n_f . Therefore, to avoid clutter we omit the subscripts on the right hand side of eq. (10). In the limit of large number of colors with N_f/N_c fixed only the partial amplitudes with $L = n_c + n_f$ contribute. These leading-color partial amplitudes receive contributions only from planar diagrams [43] and have been calculated in [24, 44–47], while $A^{(2),(1,0)}$ and $A^{(2),(0,0)}$ are known in the special all-plus helicity configuration only [37–39]. The amplitudes $\mathbf{A}^{(2),(0,0)}$, $\mathbf{A}^{(2),(-1,1)}$, $\mathbf{A}^{(2),(1,0)}$, $\mathbf{A}^{(2),(0,1)}$, $\mathbf{A}^{(2),(-1,2)}$ receive contributions from non-planar diagrams and are the new result of this work. We note that the amplitudes $A^{(2),(-1,2)}$ vanish for any helicity assignments. For convenience we also recalculate all previously known amplitudes in eq. (10).

C. Renormalization

We regularize ultraviolet (UV) and infrared (IR) divergences of loop amplitudes in the 't Hooft–Veltman scheme of dimensional regularization, setting the space-time dimensions to $D = 4 - 2\epsilon$. The UV divergences are removed by renormalization of the bare QCD coupling in the $\overline{\text{MS}}$ scheme. To achieve this we perform the following replacement in eq. (9),

$$\alpha_0 \mu_0^{2\epsilon} S_\epsilon = \alpha_s \mu^{2\epsilon} \times \quad (11)$$

$$\left(1 - \frac{\beta_0}{2\epsilon} \frac{\alpha_s}{2\pi} + \left(\frac{\beta_0^2}{4\epsilon^2} - \frac{\beta_1}{8\epsilon} \right) \left(\frac{\alpha_s}{2\pi} \right)^2 + \mathcal{O}(\alpha_s^3) \right),$$

where $S_\epsilon = (4\pi)^\epsilon e^{-\epsilon\gamma_E}$, with $\gamma_E = -\Gamma'(1)$ the Euler-Mascheroni constant, and μ_0, μ are regularization and renormalization scale respectively. The QCD β -function coefficients are

$$\beta_0 = \frac{11}{3} N_c - \frac{2}{3} N_f, \quad (12a)$$

$$\beta_1 = \frac{34}{3} N_c^2 - \frac{13}{3} N_c N_f + \frac{N_f}{N_c}. \quad (12b)$$

The renormalized amplitudes are expanded through the renormalized coupling as in eq. (9).

The remaining infrared divergences can be extracted through the universal factorization [48–51]:

$$\mathcal{R} = \mathbf{Z}(\epsilon, \mu) \mathcal{A} + \mathcal{O}(\epsilon), \quad (13)$$

where the *finite remainder* \mathcal{R} is obtained through the application of the color-space operator \mathbf{Z} . The latter is obtained [50] from the path-ordered evolution

$$\mathbf{Z}^{-1}(\epsilon, \mu) = \mathbf{P} \exp \left[\int_\mu^\infty \frac{d\mu'}{\mu'} \Gamma(\mu') \right], \quad (14)$$

of the anomalous dimension matrix

$$\Gamma(\mu) = - \sum_{(i,j)} \mathbf{T}_i \cdot \mathbf{T}_j \times \\ \frac{\gamma_{\text{cusp}}}{2} \ln \left(-\frac{s_{ij}}{\mu^2} - i0 \right) + 5\gamma^g, \quad (15)$$

where the sum runs over all pairs of external gluons, and the color operators \mathbf{T}_i act on the color representation of the i^{th} parton. For adjoint indices the action is given by $(\mathbf{T}_i^a)_{bc} = -if^{abc}$. The anomalous dimensions γ_{cusp} and γ^g can be found in [52, Appendix A]².

² We rescale them by a factor of 2 per loop to match our expansion in $\alpha_s/2\pi$ in eq. (9).

After UV and IR renormalization of amplitudes through eqs. (11) and (13) we recover expansions of eqs. (5), (9) and (10) for the finite remainders \mathcal{R} , and therefore obtain *partial finite remainders*

$$R_{\vec{h}}^{(L),(n_c,n_f)}(i_1, \dots, i_5), \quad (16)$$

which are the elementary building blocks that we focus on in this work. It is worth noting that the finite remainders contain the complete physical information about the underlying scattering process. In particular, any observable can be calculated through finite remainders (see e.g. [53]), which allows one to cancel much of the disruptions caused by the use of dimensional regularization. Finite remainders in a different IR renormalization scheme (with a different operator \mathbf{Z}) can be obtained by an additional *finite* renormalization after eq. (13). We elaborate on this in the forthcoming publication [10].

D. Generating set of finite remainders

To calculate arbitrary observable quantities we must know all partial remainders from eq. (10) in all permutations in eq. (5), with 2^5 helicity assignments for each of them. Fortunately, the combinatorial complexity can be sidestepped by mapping each partial helicity remainders onto a small generating set.

First, it is well known that in the Yang-Mills theory partial amplitudes (in the trace basis) satisfy additional identities (see e.g. [54] for a systematic study, and [55] for a recent review). We verified by a direct computation that the relations between two-loop partial amplitudes discussed in ref. [54] hold both at the level of amplitudes and finite remainders. They allow us to express $R^{(2),(0,0)}$ through sums over permutations of $R^{(2),(2,0)}$ and $R^{(2),(1,0)}$ for each helicity assignment. Interestingly, we find no linear relation among permutations of $R^{(2),(1,1)}$, $R^{(2),(0,1)}$ and $R^{(2),(-1,1)}$.

Next, we work out the generating set for each partial remainder constructively by starting with the set of all helicities and permutations, and partitioning it into the orbits under the action of the group $\mathcal{P} \otimes \mathcal{C} \otimes \Sigma_i$, where \mathcal{P} and \mathcal{C} are parity- and charge-conjugation respectively, and Σ_i is the symmetry group of the corresponding color structure in eq. (5). We can then pick one representative from each orbit, and obtain the complete set of remainders by relabeling momenta and symmetries. Let us note, that for the reasons that will become clear in section III D, we do not choose the identity permutation $\{1, 2, 3, 4, 5\}$ for all our representatives. Instead we prioritize to have uniform spinor weight for each of

the three helicity assignments $++++$ (all-plus), $+++ + -$ (single-minus), and $+++ - -$ (MHV).

For the all-plus helicity configuration we have the generating remainders

$$R_1(1^+, 2^+, 3^+, 4^+, 5^+), \quad (17a)$$

$$R_2(1^+, 2^+; 3^+, 4^+, 5^+). \quad (17b)$$

For the single-minus helicity configuration we have

$$R_1(1^+, 2^+, 3^+, 4^+, 5^-), \quad (18a)$$

$$R_2(1^+, 2^+; 3^+, 4^+, 5^-), \quad (18b)$$

$$R_2(1^+, 5^-; 4^+, 3^+, 2^+). \quad (18c)$$

Finally, for the MHV configurations we have five generating remainders,

$$R_1(1^+, 2^+, 3^+, 4^-, 5^-), \quad (19a)$$

$$R_1(1^+, 2^+, 4^-, 3^+, 5^-), \quad (19b)$$

$$R_2(1^+, 2^+; 3^+, 4^-, 5^-), \quad (19c)$$

$$R_2(1^+, 5^-; 2^+, 3^+, 4^-), \quad (19d)$$

$$R_2(5^-, 4^-; 3^+, 2^+, 1^+). \quad (19e)$$

Here we suppress the labels L, n_c, n_f , and, for better readability, we show the helicity labels as superscripts of the momentum labels.

E. NNLO hard function

To calculate the double-virtual contribution to NNLO QCD partonic cross sections one must square the helicity finite remainder $\mathcal{R}_{\vec{h}, \vec{a}}$ in eq. (5) and perform summation over color and helicity indices.

At leading order in α_s we define the function

$$\mathcal{B} = \sum_{\vec{h}, \vec{a}} \left| \mathcal{A}_{\vec{h}, \vec{a}}^{(0)} \right|^2 = N_c^3 (N_c^2 - 1) B. \quad (20)$$

We then define the *hard function* \mathcal{H} as

$$\mathcal{H} = \frac{1}{\mathcal{B}} \sum_{\vec{h}, \vec{a}} \left| \mathcal{R}_{\vec{h}, \vec{a}} \right|^2, \quad (21)$$

which can be expanded perturbatively up to $\mathcal{O}(\alpha_s^2)$ as in eq. (9). Similar to eq. (10), we can expand \mathcal{H}

in powers of N_c and N_f . Through two loops we get

$$\mathcal{H}^{(0)} = 1, \quad (22a)$$

$$\begin{aligned} \mathcal{H}^{(1)} = & N_c H^{(1),(1,0)} + \frac{1}{N_c} H^{(1),(-1,0)} \\ & + N_f H^{(1),(0,1)} + \frac{N_f}{N_c^2} H^{(1),(-2,1)}, \end{aligned} \quad (22b)$$

$$\begin{aligned} \mathcal{H}^{(2)} = & N_c^2 H^{(2),(2,0)} + H^{(2),(0,0)}, \\ & + N_f \sum_{n_c \in \{1, -1, -3\}} N_c^{n_c} H^{(2),(n_c,1)}, \\ & + N_f^2 \sum_{n_c \in \{0, -2, -4\}} N_c^{n_c} H^{(2),(n_c,2)}. \end{aligned} \quad (22c)$$

Here again only the functions $H^{(L),(n_c, n_f)}$ with $L = n_c + n_f$ contribute in the leading-color approximation.

To perform the summations in eq. (21) we use the maps inverse to the ones that were used in the previous section to construct the generating set of finite remainders. It is worth noting that the polynomial expansion in N_c and N_f given in eq. (22) holds only when identities between partial remainders are correctly taken into account.

III. ANALYTIC RECONSTRUCTION

We now discuss the computation of the finite remainders (13). They can be represented as a linear combination of transcendental integral functions h_i and rational coefficient functions r_i ,

$$R = \sum_i r_i h_i. \quad (23)$$

For the integral functions h_i , we employ the set of non-planar pentagon functions from ref. [15]. The rational coefficient functions are the central result of this paper and we obtain them via analytic reconstruction, i.e. we start with an ansatz for the rational coefficient functions r_i and determine its parameters from exact numerical evaluations of the remainder over prime fields. The reconstruction cost is dominated by the time of sampling the remainders. This motivates us to search for a strategy to constrain the ansatz using physics arguments and reduce its free parameters. We will now discuss the details of this computation.

A. Numerical sampling

For numerical amplitude evaluations in a finite field we use the program CARAVEL [34], which implements the multi-loop numerical unitarity method

[31–33]. In this approach amplitudes are reduced to a set of master integrals by matching numerical evaluations of generalized unitarity cuts to a parametrization of the loop integrands. For the five-gluon process we use the recently obtained parametrization [35], which we extend in loop-momentum degree to match the corresponding dependence of the gluon cut diagrams. Furthermore, we extended the set of planar unitarity cuts to non-planar diagrams which are required for subleading-color partial amplitudes. We generated the cut diagrams with `qgraf` [56] and arranged them into a hierarchy of cuts with a private code. We matched the cuts evaluated through color-ordered tree amplitudes to the amplitude definitions in section IIB, by employing the unitarity based color decomposition [57, 58]. We extracted the ϵ -dependence of cuts that originates from the state sums in loops through the dimensional reduction method [59, 60].

With these extensions CARAVEL now computes the integral coefficients r_i of five-gluon partial amplitudes up to two loops, given a kinematic point and a choice of polarization labels for the external gluons.

Analytic expressions for the coefficient functions r_i can then be reconstructed using multivariate functional reconstruction techniques [16, 17] (see also recent refs. [18–20, 25]) based on Newton and Thiele’s interpolation algorithms. However, our approach is in fact closer to the ansatz-based approach of refs. [21, 26]. This approach constructs an ansatz for the rational integral coefficients r_i , which is constrained by information from the neighborhood of their singularities. Nevertheless, here we differ even from this approach in that we use information about the residues to build linear transformations of rational functions r_i to bases of functions \tilde{r}_i with a simplified pole structure and fewer ansatz parameters. This basis change is determined numerically and simplifies the subsequent ansatz construction and parameter determination.

We will require two types of numerical evaluations for the remainder functions:

1. Random phase-space points: these are N randomly generated phase-space points which we label by the superscript n . We represent these points in terms of sets of spinor variables,

$$\{\{\lambda_1^n, \dots, \lambda_5^n, \tilde{\lambda}_1^n, \dots, \tilde{\lambda}_5^n\}\}_{n=1, N}. \quad (24)$$

They are subject to momentum conservation $\sum_i \lambda_i^n \tilde{\lambda}_i^n = 0$.

2. A family of (anti-)holomorphic slices: these are $\tilde{N} < N$ holomorphic slices [23, 35, 61] associated to a subset of the random phase-space

points (24),

$$\lambda_i^{\tilde{n}}(t) = \lambda_i^{\tilde{n}} + t c_i^{\tilde{n}} \eta^{\tilde{n}}, \quad \tilde{\lambda}_i^{\tilde{n}}(t) = \tilde{\lambda}_i^{\tilde{n}},$$

$$\sum_{i=1}^5 c_i^{\tilde{n}} \tilde{\lambda}_i^{\tilde{n}} = 0. \quad (25)$$

Here the reference spinor $\eta^{\tilde{n}}$ is chosen randomly. The label \tilde{n} runs over \tilde{N} values. Similarly we will use anti-holomorphic slices which are obtained from (25) by swapping $\lambda_i^{\tilde{n}} \leftrightarrow \tilde{\lambda}_i^{\tilde{n}}$ and $\eta^{\tilde{n}} \rightarrow \tilde{\eta}^{\tilde{n}}$.

B. Coefficient-function basis

We now identify a basis of coefficient functions r_i based on a measure for the functions' complexity. We start from the general form of the rational coefficient functions in spinor variables,

$$r_i = \frac{\mathcal{N}_i(\lambda, \tilde{\lambda})}{\prod_j \mathcal{D}_j^{q_{ij}}(\lambda, \tilde{\lambda})}. \quad (26)$$

The denominator factors \mathcal{D}_j are given by the symbol alphabet with integer exponents q_{ij} [24]. Computing r_i amounts to determining the q_{ij} and all parameters in the numerator polynomial \mathcal{N}_i . While it is straightforward to determine q_{ij} (see below) it is non-trivial to determine \mathcal{N}_i because of the typically large polynomial degree. Consequently, a useful measure of complexity is the mass dimension of \mathcal{N}_i , which is linked to the number of parameters the polynomial depends on.

Simple dimensional analysis allows us to determine the mass dimension and spinor weights of the numerators \mathcal{N}_i , from those of the polynomials \mathcal{D}_j , the data q_{ij} and the overall mass dimension and spinor weights of the helicity remainder. Consequently, we only need to determine the exponents q_{ij} , which we compute following the univariate-slice reconstruction [24] in spinor-helicity variables [61] (see also refs. [23, 35]). Here the remainder functions are reconstructed on a single holomorphic and a single anti-holomorphic slice (25), and subsequently the denominators are matched to products of the letter polynomials $\mathcal{D}_j(t)$. This uniquely fixes the exponents q_{ij} for each function r_i .

For the five-gluon finite remainders we observe that the set of denominator factors contains the 35 elements,

$$\mathcal{D} = \{ \langle ij \rangle, [ij], \langle i|j+k|l \rangle, \dots \} \quad (27)$$

where the set runs over all independent permutations of the spinor strings/brackets. We also note that no coefficient in the finite remainder has a tr_5

singularity. From the q_{ij} we can immediately deduce the mass dimension of the numerators \mathcal{N}_i .

Our next goal is to determine a minimal function basis for the set of coefficient functions r_i in order to reduce the number of rational functions r_i that must to be constructed [60]. To this end, we exploit the freedom in our choice of basis functions and select a basis containing numerators with the lowest mass dimensions. We express the linear dependent r_i through the basis as

$$r_i = \sum_{j \in \text{basis}} r_j M_{ji}, \quad (28)$$

where M_{ij} is a constant rectangular matrix. At this point we do not have analytic expressions for the r_i available and we require a numerical method to identify linear dependence of functions. This is achieved using a set of random evaluations (24) [60, 62], which allows to associate vectors \vec{r}_i of function values to each r_i . A function basis is then identified by identifying a basis in the vector space of function values $\vec{r}_i = \sum_{j \in \text{basis}} \vec{r}_j M_{ji}$ by linear algebra. After this step, we arrive at the form of the remainder,

$$R = \sum_{j \in \text{basis}, i} r_j M_{ji} h_i. \quad (29)$$

Obtaining the analytic form of the remainder now amounts to computing the set $\{r_i\}_{i \in \text{basis}}$.

C. Basis change

So far we have selected a convenient basis of functions $\{r_i\}_{i \in \text{basis}}$. Next, we will exploit universal properties of the functions' poles, namely correlations between residues, to construct linear transformations to a simpler basis of functions, which we will denote by \tilde{r}_i . ('Simpler' again refers to the \tilde{r}_i functions having numerators with lower mass dimension than the ones of the r_i .) A basis change of this type was used already some time ago in ref. [24] and a detailed discussion of the algorithm will be presented in the forthcoming paper [36]. Here we summarize the main steps. The reason that such linear combinations exist, stems from the fact that many poles (at zeros of the \mathcal{D}_i) are spurious and cancel in the remainders. (Examples of spurious-pole denominators are spinor strings $\langle i|j+k|l \rangle$, as well as higher-order spinor products $[ij]$ and $\langle ij \rangle$ which do not contribute to factorization poles.) Such cancellations require that the residues of distinct r_i are linearly related; only in this way they may cancel when multiplied with (degenerate) transcendental functions h_i evaluated on the respective singular surfaces.

We now discuss the simplifying basis change from the functions r_i to \tilde{r}_i for a given remainder. We start

by defining our requirement for a constant linear basis change O_{ij} ,

$$\tilde{r}_i = \sum_{j \in \text{basis}} O_{ij} r_j. \quad (30)$$

Our objective is to ensure that the mass dimension of all new numerators $\tilde{\mathcal{N}}_i$,

$$\tilde{r}_i = \frac{\tilde{\mathcal{N}}_i(\lambda, \tilde{\lambda})}{\prod_j \mathcal{D}_j^{\tilde{q}_{ij}}(\lambda, \tilde{\lambda})}, \quad (31)$$

is lower than those in the original least common denominator (LCD) form (26),

$$\dim(\tilde{\mathcal{N}}_i) < \dim(\mathcal{N}_i) \quad i \in \text{basis} \quad (32)$$

where $\dim(\mathcal{N}_i)$ denotes the mass dimension of numerator \mathcal{N}_i .

The property we use is that the mass dimension is linked to the exponents \tilde{q}_{ij} . We are thus lead to consider the residues of the coefficient functions on the zeros of the denominator factors \mathcal{D}_j . To this end we use a family of holomorphic univariate slices (25) and obtain a univariate representation of the coefficient functions $\tilde{r}_i(t)$. Near a single zero t_k of one of the denominator factors

$$\mathcal{D}_k(t_k) = 0, \quad (33)$$

we obtain a formal Laurent series

$$r_i(t) = \sum_{m=1}^{q_{ik}} \frac{e_{im}^k}{(t-t_k)^m} + \mathcal{O}((t-t_k)^0), \quad (34)$$

with e_{im}^k being functions of the external kinematics. The e_{im}^k will be referred to as codimension-one residues. To write the above equation (34) in a more uniform way, we introduce the maximal pole degree of a given factor \mathcal{D}_k ,

$$q_k = \max_{i \in \text{basis}} [q_{ik}]. \quad (35)$$

At the same time we introduce vanishing residues,

$$e_{im}^k = 0 \quad \text{for} \quad q_{ik} < m \leq q_k, \quad (36)$$

and rewrite (34) as,

$$r_i(t) = \sum_{m=1}^{q_k} \frac{e_{im}^k}{(t-t_k)^m} + \mathcal{O}((t-t_k)^0). \quad (37)$$

In this way the summation is independent of the residue function and the degree of the pole is encoded in the vanishing of residues.

Equipped with this notation, we now return to the discussion of the constant transformation matrix O_{ij} . We will now constrain the matrix, such

that some of the leading residues vanish for the new basis \tilde{r}_i . This is equivalent to lowering the respective pole degrees \tilde{q}_{ij} (and consequently the numerators' mass dimensions), which is what we aimed to achieve in the first place. The Laurent expansion of the functions \tilde{r}_i depends linearly on the data of the Laurent expansion of r_i ,

$$\tilde{r}_i(t) = \sum_{m=1}^{q_k} \frac{\tilde{e}_{im}^k}{(t-t_k)^m} + \mathcal{O}((t-t_k)^0), \quad (38)$$

$$\tilde{e}_{im}^k = \sum_{j \in \text{basis}} O_{ij} e_{jm}^k. \quad (39)$$

Consequently, we can choose the basis change O_{ij} in such a way, that the leading residue vanishes, effectively reducing the power of the leading pole,

$$\sum_{j \in \text{basis}} O_{ij} e_{jq_k}^k = 0. \quad (40)$$

We find that the requirement for a good basis change is that the columns of the matrix O_{ij} are in the kernel of the leading residue functions. Independently, we also have to ensure that the basis change is invertible. Given this property, the pole degrees of the \tilde{r}_i are reduced.

Finally, we adjust the criterion for the fact that we do not have analytic expressions for the residue functions available. We follow the strategy of ref. [60, 62] (see also section III B). We repeat the above construction for \tilde{D} holomorphic slices (25) (labeled by \tilde{n}) and obtain a representation of the residue functions e_{im}^k as vectors of their function values

$$\vec{e}_{im}^k = \{e_{im}^k(t_k^1), \dots, e_{im}^k(t_k^{\tilde{D}})\}. \quad (41)$$

The linear constraint for the basis change O_{ij} is upgraded to,

$$\sum_{j \in \text{basis}} O_{ij} \vec{e}_{jq_k}^k = 0, \quad (42)$$

and relies solely on numerical input. The required number \tilde{D} of slices is given by the dimension of the largest vector space of codimension-one residues $e_{jq_k}^k$.

So far we were concerned with removing the leading singularity associated to the pole labeled by k . In practice we impose the linear constraint (42) for multiple residues simultaneously. This includes originally subleading residues, if they transform into leading residues following the cancellation of the previous leading ones. In fact, for the most complicated function k runs over up to 40 residues. Furthermore, we find it convenient to derive the basis change by considering one function \tilde{r}_i at a time, which amounts

to constructing O_{ij} row by row. We start from the simplest functions, progressing towards the most complex ones. In certain cases, the computation for the last rows of O_{ij} was unnecessary, as these functions were derived through symmetries (as discussed below) or other partial remainders. The impact of the basis change is presented in table II in terms of LCD ansatz sizes.

Using basis changes that decorrelate the functions poles we have achieved much simplified coefficient functions prior to performing a prohibitively expensive reconstruction. The effect is somewhat similar to what was achieved by univariate partial fractioning by a suitable variable [22, 23, 63]. However, we avoid introducing new spurious denominators, and in addition the order of unphysical poles is systematically reduced. Both effects are expected to lead to much improved numerical stability. Moreover, we also note that, following the change in the set of basis functions, further simplification may be achieved by a partial-fraction decomposition, either by the semi-numerical slicing techniques just mentioned, or through the purely numerical approach of refs. [21, 26].

D. Analytic reconstruction and simplification

We are now in a position to reconstruct the coefficient functions. We do this by constructing an ansatz matching the pole structure of the final LCD form (31). Given previous experience, we further simplify the ansatz by removing terms with more than one $\langle i|j+k|i\rangle$ -factors in the denominator [35]. For example, we expect (and verify) \mathcal{N} to be such that the following type of equality holds

$$\frac{\mathcal{N}}{(4|1+5|4|^2\langle 5|3+4|5|^2)} = \frac{\mathcal{N}_a}{(4|1+5|4|^2)} + \frac{\mathcal{N}_b}{\langle 5|3+4|5|^2} \quad (43)$$

irrespective of what other denominator factors appear and of the degree of the spinor chains. This allows us to make the ansatz in terms of the two lower-degree numerator polynomials $\mathcal{N}_{a,b}$ instead of \mathcal{N} . Constructing an ansatz for the numerator polynomial can be non trivial. We build ansätze for the numerator polynomials in terms of independent monomials of spinor brackets, which have both the right mass dimension and little group weights. Mathematically, this amounts to the enumeration of members of a polynomial quotient ring, subject to irreducibility by a Gröbner basis and degree bounds [21, section 2.2]. The ansatz construction relies on the open-source programs `Singular` [64], for the Gröbner basis computation, and `OR-tools` [65], for the linear

programming. Finally, we determine the numerator polynomials by solving linear systems for a sufficient number of random evaluations (24).

When reconstructing the coefficient functions of all remainders of the generating sets (17), (18) and (19), we find it most effective to reconstruct remainder functions in bunches of the same spinor weight. Furthermore, we find it most effective to reconstruct denominators of lower mass dimension first. We also observe that permuting the momentum assignments of the functions \tilde{r}_i that yield the same spinor weight often yields linearly independent coefficient functions. We thus, after each newly reconstructed coefficient function, ensure that the set of functions is closed under all momentum permutations that leave the little-group weights unchanged. This ensures that information is recycled among different partials, and that the symmetries of amplitudes are exploited. Numerically, the closure of the space of functions is conveniently checked by adding all permutations and evaluating them on the random phase-space points (24). We then filter out redundant ones via Gaussian elimination.

After the reconstruction of the function coefficients is complete, we simplify the final results considering each of the three helicity sets individually. In fact, we perform a further basis change on the vector space obtained from the union of all remainders. We determine a simple basis for this space, by placing the chosen basis functions in global, or failing that local, minima in the space of possible denominator powers [35]. Finally, the basis functions are then partial fractioned following the approach of refs. [21, 26].

We display the set of all coefficient functions in appendices A to C.

E. Implementation

To perform the reconstruction, for the most complicated remainder, we use roughly 35,000 numerical samples. Most of these samples are points on slices needed to perform the basis change, while around 5,000 are random phase-space points. All rational functions are fitted with a single finite field. This is possible thanks to the size of the rational numbers appearing in the basis, with the largest ones not exceeding 2 digits. Initially the matrices M_{ij} are obtained in a finite field. To lift the matrices M_{ij} from a finite field to rational numbers we require, on the first finite field value, as many samples as the dimension of the vector space, while subsequent finite field values requires roughly a factor of 5 fewer samples for each iteration. In the end, a single evaluation with a finite field value not employed

Gluon helicities	Vector-space dimension	Generating set size
+++ ++	24	3
+++ +-	440	33
+++ --	937	115

Table I: For each helicity configuration, this table shows the dimension of the vector space of rational functions, and the number of functions in the generating set that spans the space upon closure under the symmetries of the helicity vector.

in the reconstruction is used as a check.

Finally, we summarize software packages used in the analytic reconstruction. We take advantage of hardware acceleration on NVIDIA GPUs with the private code `linac` (LINear Algebra with CUDA), which we use to solve linear systems over a finite fields for the ansatz coefficients, and to handle the vector spaces of rational functions. We use `lips` and `pyadic` [66] for the generation and manipulations of phase-space points defined in terms of spinors, and for numerical evaluations of spinor-helicity functions.

IV. RESULTS

We express remainders in terms of three rational-function bases. The function bases are obtained from a generating set of spinor-helicity functions and symmetry operations. We denote the generating functions as $\tilde{r}_i^{h_4 h_5}$, with h_4 and h_5 labeling the three helicity configuration: all-plus (\tilde{r}_i^{+++}), single-minus (\tilde{r}_i^{+-}), and MHV (\tilde{r}_i^{--}). The respective basis functions are given in appendices A to C. The functions themselves are expressed in terms of spinor-helicity variables, and symmetry operations. The latter take the form

$$(12345 \rightarrow \pm\sigma_1\sigma_2\sigma_3\sigma_4\sigma_5) \quad (44)$$

where “ $-$ ” denotes that the expression with the permuted labels should be subtracted. For example,

$$r(1, 2, 3, 4, 5) + (12345 \rightarrow 45321) = \quad (45)$$

$$r(1, 2, 3, 4, 5) + r(4, 5, 3, 2, 1), \quad (46)$$

$$r(1, 2, 3, 4, 5) + (12345 \rightarrow -45321) = \quad (47)$$

$$r(1, 2, 3, 4, 5) - r(4, 5, 3, 2, 1). \quad (48)$$

Within a rational function, the employed convention is to apply the (anti-)symmetrization to all terms preceding the mapping [26, section 4.3].

To obtain the function basis from the generating functions, the set needs to be closed under the

symmetries of the little group weights. These are $\mathcal{S}_5(1, 2, 3, 4, 5)$, $\mathcal{S}_4(1, 2, 3, 4)$ and $\mathcal{S}_3(1, 2, 3) \otimes \mathcal{S}_2(4, 5)$, for all-plus, single-minus and MHV configurations, respectively (here $\mathcal{S}_n(1, \dots, n)$ denotes the group of permutations of the elements $\{1, \dots, n\}$). Table I shows the dimensions of the three vector spaces, and the number of generating spinor-helicity expressions in the chosen basis. The dimensions of the vector spaces are uniquely defined, in the sense that they are the smallest spaces that are both closed under the symmetries and that span all coefficients in the required partials. The number of generating functions is representation dependent.

We note that the overlap between the rational-function spaces of the different partials is significant. This can be observed by comparing the sizes of the vector spaces in table II, to that of their union, closed under $\mathcal{S}_3(1, 2, 3) \otimes \mathcal{S}_2(4, 5)$, in table I, in spite of the fact that the spaces of partials are not closed under all symmetries of the phase weights.

The remaining helicity configurations are obtained by re-assigning momentum labels and/or parity conjugation. However, some of the permutation of eq. (5) will involve exchanges between momenta in the initial and final state. This encompasses non-trivial analytic continuation, which we perform following ref. [5]. More explicitly, the action of permutation σ on a finite remainder R is given by

$$\sigma \circ R = \sigma \circ (\tilde{r}_i M_{ij} h_j) = (\sigma \circ \tilde{r})_i M_{ij} Q_{jk} h_k \quad (49)$$

$$= (\sigma \circ \tilde{r})_i M'_{ij} h_j. \quad (50)$$

Here we rely on the closure of the pentagon functions under permutations [15]. The analytic continuation therefore amounts to simply obtaining a matrix M'_{ij} for each required permutation. In practice, these matrices are obtained by permuting the legs in the master integrals only, and then re-mapping them to pentagon functions.

A. Ancillary files

We provide expressions for the finite remainders of all independent partial amplitudes through two loops in the decomposition of eqs. (5), (9) and (10) in [67]. For each helicity configuration, all-plus, single-minus and MHV, we organize the results in terms of two global bases, valid for all partials and crossings, in the files

1. `basis_transcendental`,

2. `basis_rational`.

The constant matrices M_{ij} of rational numbers are partial remainder, and permutation specific. They

Helicity remainder	dim(VS(\mathcal{R}))	LCD ansatz size	
		before basis change	after basis change
$R_{++++}^{(2),(2,0)}$	31	21,910	N/A
$R_{++-+-}^{(2),(2,0)}$	54	54,148	N/A
$R_{++++}^{(2),(1,0)}$	274	163,635	14,093
$R_{+---}^{(2),(1,0)}$	270	241,156	14,552
$R_{--+++}^{(2),(1,0)}$	203	82,180	25,620
$R_{++++}^{(2),(1,1)}$	31	21,910	N/A
$R_{++-+-}^{(2),(1,1)}$	54	54,148	N/A
$R_{++++}^{(2),(0,1)}$	226	118,880	4,108
$R_{+---}^{(2),(0,1)}$	240	209,018	N/A
$R_{--+++}^{(2),(0,1)}$	157	76,845	8,840
$R_{++++}^{(2),(-1,1)}$	25	5,320	N/A
$R_{++-+-}^{(2),(-1,1)}$	35	9,384	N/A

Table II: For each partial amplitude, this table shows the dimension of the vector space of rational functions, and ansatz size in LCD form of the most complicated function in the basis, before and after basis change. In the cases denoted by N/A the basis change was not required.

are organized in subfolders labeling the partial remainders from subsection IID, with the notation

$$\{\vec{h}\}_{\{L\}L_Nc\{n_c\}Nf\{n_f\}/},$$

where \vec{h} , L , n_c and n_f refer to helicities, number of loops, number of N_c powers and number of N_f powers, as defined earlier in the paper. For completeness of the ancillaries, we also provide information about permutations and color structures of the partials in the file `amp_info`.

The matrices themselves are stored in the files

$$\text{rational_matrix}_{\{\text{permutation}\}},$$

where it is understood that this permutation has to be combined with that of each partial as defined in subsection IID and in `amp_info`. The order of the permutations matters, with those defined in IID taking precedence.

B. Validation

Our computation incorporates multiple internal consistency checks at various stages. In constructing the finite remainders, we ensure the cancellation of poles in the dimensional regulator ϵ at every kinematic point. Further validation of the finite field reconstruction occurs at an independent kinematic

point, not utilized for the reconstruction, and with a distinct value of the prime.

We found agreement with the numerical evaluations for the helicity- and color-summed squared remainders in the leading-color approximation [5]. Furthermore, we conduct additional checks through independent computations in full color. We compared the one-loop hard functions against numerical evaluations by `BlackHat` [68] and found agreement. At two loops we performed verification against the full-color all-plus calculation [37], and the validation of the evaluations provided in appendix D with an independent computation [40, 69].

C. Numerical evaluation

We implement our analytic results for the partial helicity remainders, as well as for the NNLO hard function defined in eq. (21) in the C++ library `FivePointAmplitudes` [70], which employs `PentagonFunctions++` [15, 71, 72] for numerical evaluation of the transcendental integral functions. This allows us to ensure the stability of numerical evaluations via the rescue system developed in ref. [5]. We achieve excellent numerical performance, with a single numerical evaluation of the two-loop hard function taking a few seconds in double precision on a personal desktop computer. The aver-

age evaluation time per phase-space point on cluster nodes over the phase-space of ref. [5] is around 8s with the rescue system enabled. For comparison, the average evaluation time for the leading-color contribution only is around 1.6s with the same setup.

V. CONCLUSIONS

In this work we computed the two-loop five-gluon helicity amplitudes in QCD. The amplitudes are uniformly represented in terms of a basis of rational coefficient functions, transcendental functions and constant matrices of rational numbers that link the two. We achieved an unprecedented level of simplicity in the basis of coefficient functions, by identifying a distinguished basis of functions based on their singularity structure. However, it has to be noted that significant complexity still remains in the transcendental functions and in the mentioned matrices of rational numbers. This observation raises an intriguing possibility of a more physically motivated basis of transcendental functions, rooted in the cancellation of spurious singularities, that is, in the amplitudes' locality. Further exploration into this avenue remains an intriguing direction for future research.

In terms of phenomenological applications, the significance of our result becomes particularly evident when considering not just three-jet production at NNLO, but also two-jet at N³LO in hadron collisions. In fact, the latter will require integrating the provided expressions in unresolved phase-space configurations. We expect our compact basis of rational coefficient functions to benefit both precision and stability of such computations.

Finally, the simplicity achieved in the present computation is not confined to the specific channel under consideration, nor are the techniques employed specific to five-point massless kinematics. Analogous results for the quark channels of three-jet production will follow shortly in a separate publication, and preliminary studies show similar benefits in tackling processes involving more challenging kinematics, such as five-point one-mass. In summary, we believe that the form of the rational coefficient functions, which directly benefits phenomenological studies, deserves further studies concerning the mathematical structure of scattering amplitudes, and may open new paths to precision predictions for multi-scale scattering processes at particle colliders.

ACKNOWLEDGMENTS

First and foremost, we gratefully acknowledge Ben Page for stimulating conversations and for collabo-

ration on the basis-change algorithm [36] that we applied in this paper. We thank Thomas Gehrmann for interesting discussions. We thank Johannes Schlenk for discussions and comments on the manuscript. Finally, we thank Bakul Agarwal, Federico Buccioni, Federica Devoto, Giulio Gambuti, Andreas von Manteuffel, Lorenzo Tancredi for the numerical comparison of the reference values which are displayed in appendix D. We gratefully acknowledge the computing resources provided by the Paul Scherrer Institut (PSI) and the University of Zurich (UZH). V.S. has received funding from the European Research Council (ERC) under the European Union's Horizon 2020 research and innovation programme grant agreement 101019620 (ERC Advanced Grant TOPUP). G.D.L.'s work is supported in part by the U.K. Royal Society through Grant URF\R1\20109.

Appendix A: Five-gluon all-plus basis functions

$$\tilde{r}_1^{++} = \frac{[45]^2}{\langle 12 \rangle \langle 13 \rangle \langle 23 \rangle}$$

$$\begin{aligned} \tilde{r}_2^{++} = & \frac{-\langle 14 \rangle \langle 24 \rangle \langle 25 \rangle [25] \langle 35 \rangle [45]}{\langle 12 \rangle^2 \langle 15 \rangle \langle 23 \rangle \langle 34 \rangle^2 \langle 45 \rangle} + \\ & \frac{[24][35]}{\langle 12 \rangle \langle 15 \rangle \langle 34 \rangle} + \\ & (12345 \rightarrow 23451) + (12345 \rightarrow 34512) + \\ & (12345 \rightarrow 45123) + (12345 \rightarrow 51234) \end{aligned}$$

$$\begin{aligned} \tilde{r}_3^{++} = & \frac{\text{tr}_5(1234)}{\langle 12 \rangle \langle 15 \rangle \langle 25 \rangle \langle 34 \rangle^2} + \\ & (12345 \rightarrow 12453) + \\ & (12345 \rightarrow 12534) \end{aligned}$$

Appendix B: Five-gluon single-minus basis functions

$$\begin{aligned}
\tilde{r}_1^{+-} &= \frac{[34]^3}{\langle 12 \rangle^2 [35] [45]} & \tilde{r}_{18}^{+-} &= \frac{-15 \langle 45 \rangle [13] \langle 15 \rangle}{\langle 13 \rangle \langle 14 \rangle \langle 24 \rangle^2} + \\
& & & \frac{\langle 45 \rangle^2 [34] [23]}{\langle 14 \rangle^2 \langle 24 \rangle^2 [24]} \\
\tilde{r}_2^{+-} &= \frac{\langle 45 \rangle [23] \langle 15 \rangle}{\langle 14 \rangle^3 \langle 23 \rangle} & \tilde{r}_{19}^{+-} &= \frac{-3 \langle 23 \rangle \langle 25 \rangle \langle 35 \rangle [12]}{\langle 12 \rangle \langle 23 \rangle^2 \langle 34 \rangle^2} + \\
& & & \frac{-2 \langle 25 \rangle^2 \langle 35 \rangle [12]}{\langle 12 \rangle \langle 23 \rangle^2 \langle 34 \rangle \langle 45 \rangle} \\
\tilde{r}_3^{+-} &= \frac{\langle 25 \rangle [23] \langle 35 \rangle}{\langle 14 \rangle^2 \langle 23 \rangle^2} & \tilde{r}_{20}^{+-} &= \frac{12 \langle 25 \rangle [14] \langle 15 \rangle}{\langle 12 \rangle \langle 14 \rangle \langle 23 \rangle^2} + \\
& & & \frac{\langle 25 \rangle \langle 45 \rangle [14] [24]}{\langle 12 \rangle [12] \langle 14 \rangle \langle 23 \rangle^2} \\
\tilde{r}_4^{+-} &= \frac{[45] \langle 25 \rangle^3}{\langle 12 \rangle^2 \langle 23 \rangle^2 \langle 24 \rangle} & \tilde{r}_{21}^{+-} &= \frac{5 \langle 35 \rangle^2 [45] [23]^2}{\langle 13 \rangle^2 \langle 34 \rangle^2 [34] [35]} + \\
& & & \frac{17 \langle 35 \rangle^2 [24] [23]}{\langle 13 \rangle^2 \langle 34 \rangle^2 [34]} \\
\tilde{r}_5^{+-} &= \frac{\langle 25 \rangle^2 [12]}{\langle 12 \rangle \langle 23 \rangle \langle 24 \rangle \langle 34 \rangle} & \tilde{r}_{22}^{+-} &= \frac{[35] \langle 45 \rangle^3 [24] \langle 15 \rangle}{\langle 14 \rangle^3 \langle 24 \rangle \langle 34 \rangle [34] \langle 35 \rangle} + \\
& & & \frac{8 \langle 45 \rangle^3 [24]}{\langle 14 \rangle^2 \langle 24 \rangle \langle 34 \rangle \langle 35 \rangle} \\
\tilde{r}_6^{+-} &= \frac{[25] \langle 25 \rangle^3}{\langle 12 \rangle^2 \langle 23 \rangle \langle 24 \rangle \langle 34 \rangle} & \tilde{r}_{23}^{+-} &= \frac{-\langle 35 \rangle \langle 25 \rangle^2 [12] [45]}{\langle 12 \rangle \langle 23 \rangle^3 [25] \langle 45 \rangle} + \\
& & & \frac{-10 \langle 35 \rangle \langle 25 \rangle^2 [12]}{\langle 12 \rangle \langle 23 \rangle^2 \langle 34 \rangle \langle 45 \rangle} \\
\tilde{r}_7^{+-} &= \frac{\langle 24 \rangle \langle 25 \rangle \langle 13 \rangle \langle 15 \rangle [34]}{\langle 12 \rangle^4 \langle 34 \rangle^2} & \tilde{r}_{24}^{+-} &= \frac{3 \langle 34 \rangle \langle 35 \rangle \langle 25 \rangle^2 [14] [24]}{[12] \langle 14 \rangle \langle 15 \rangle \langle 23 \rangle^4} + \\
& & & \frac{\langle 35 \rangle \langle 45 \rangle [14] [24]}{[12] \langle 13 \rangle \langle 14 \rangle \langle 23 \rangle^2} \\
\tilde{r}_8^{+-} &= \frac{[15] \langle 35 \rangle^2 \langle 25 \rangle^2}{\langle 15 \rangle \langle 23 \rangle^3 \langle 24 \rangle \langle 34 \rangle} & \tilde{r}_{25}^{+-} &= \frac{\langle 34 \rangle \langle 35 \rangle \langle 25 \rangle [14] [34]}{\langle 13 \rangle [13] \langle 14 \rangle \langle 23 \rangle^3} + \\
& & & \frac{-5 \langle 35 \rangle \langle 45 \rangle [14]^2 [23]}{[12] \langle 13 \rangle [13] \langle 14 \rangle \langle 23 \rangle^2} \\
\tilde{r}_9^{+-} &= \frac{[23] \langle 45 \rangle [34] \langle 25 \rangle}{\langle 12 \rangle \langle 14 \rangle \langle 24 \rangle^2 [24]} & \tilde{r}_{26}^{+-} &= \frac{5 \langle 34 \rangle \langle 35 \rangle [45] \langle 25 \rangle^3 [24]}{\langle 12 \rangle \langle 15 \rangle \langle 23 \rangle^4 [25] \langle 45 \rangle} + \\
& & & \frac{4 \langle 35 \rangle \langle 25 \rangle^2 [12] [45]}{\langle 12 \rangle \langle 23 \rangle^3 [25] \langle 45 \rangle} \\
\tilde{r}_{10}^{+-} &= \frac{\langle 45 \rangle [14] [23] \langle 15 \rangle}{\langle 14 \rangle^2 \langle 23 \rangle \langle 1|2+3|1} \frac{[12] [34] \langle 25 \rangle^2}{\langle 12 \rangle \langle 23 \rangle \langle 24 \rangle \langle 2|1+5|2}} & \tilde{r}_{27}^{+-} &= \frac{-[45] \langle 15 \rangle \langle 25 \rangle^3 [12]}{\langle 12 \rangle^2 \langle 23 \rangle^2 \langle 45 \rangle \langle 2|1+5|2}} + \\
& & & \frac{-3 [34] \langle 25 \rangle \langle 45 \rangle \langle 35 \rangle [25]}{\langle 12 \rangle^2 \langle 34 \rangle^2 \langle 2|1+5|2}} \\
\tilde{r}_{11}^{+-} &= \frac{\langle 25 \rangle^2 \langle 45 \rangle [34] [23]}{\langle 12 \rangle \langle 15 \rangle \langle 24 \rangle^3 [24]} & \tilde{r}_{28}^{+-} &= \frac{\langle 25 \rangle [12]^2 [34]}{\langle 12 \rangle [15] \langle 34 \rangle \langle 2|1+5|2}} + \\
& & & (12345 \rightarrow -43215) + \\
& & & \frac{[12] [14] [34]}{\langle 12 \rangle [15] \langle 34 \rangle [45]} \\
\tilde{r}_{12}^{+-} &= \frac{\langle 35 \rangle^2 \langle 25 \rangle [25] [14]}{[12] \langle 13 \rangle \langle 14 \rangle \langle 23 \rangle^3} & \tilde{r}_{29}^{+-} &= \frac{[35] \langle 45 \rangle^3 \langle 15 \rangle^2 [45]}{\langle 14 \rangle^4 \langle 23 \rangle \langle 24 \rangle [34] \langle 35 \rangle} + \\
& & & \frac{-4 [35] \langle 45 \rangle^3 \langle 13 \rangle \langle 15 \rangle}{\langle 14 \rangle^4 \langle 23 \rangle \langle 24 \rangle \langle 35 \rangle} + \\
& & & \frac{4 \langle 45 \rangle^3 \langle 12 \rangle [24]}{\langle 14 \rangle^3 \langle 23 \rangle \langle 24 \rangle \langle 35 \rangle} \\
\tilde{r}_{13}^{+-} &= \frac{\langle 45 \rangle [14]^2 [23] \langle 15 \rangle}{\langle 14 \rangle \langle 23 \rangle \langle 1|2+3|1} \frac{[12] [34] \langle 25 \rangle^2}{\langle 12 \rangle \langle 23 \rangle \langle 24 \rangle \langle 2|1+5|2}} & \tilde{r}_{30}^{+-} &= \frac{-2 [12] [23] \langle 25 \rangle^2 [24] [34]}{\langle 12 \rangle \langle 2|1+5|2|^3} + \\
& & & \frac{-[12] \langle 25 \rangle \langle 45 \rangle [24] [34]}{\langle 12 \rangle \langle 34 \rangle \langle 2|1+5|2|^2} + \\
& & & \frac{2 \langle 35 \rangle \langle 45 \rangle [12] [34]}{\langle 12 \rangle \langle 34 \rangle^2 \langle 2|1+5|2}} \\
\tilde{r}_{14}^{+-} &= \frac{\langle 35 \rangle^2 \langle 25 \rangle [25] [34]}{\langle 12 \rangle \langle 13 \rangle \langle 23 \rangle^2 [23] \langle 34 \rangle} & \tilde{r}_{31}^{+-} &= \frac{-2 \langle 35 \rangle \langle 25 \rangle [34]}{\langle 12 \rangle^2 \langle 23 \rangle \langle 34 \rangle} + \\
& & & \frac{2 \langle 45 \rangle [14] [34] \langle 15 \rangle}{\langle 12 \rangle^2 \langle 34 \rangle \langle 1|2+3|1}} + \\
& & & \frac{3 [23] \langle 35 \rangle [13] [14] \langle 15 \rangle}{\langle 14 \rangle \langle 23 \rangle \langle 1|2+3|1} + \\
& & & \frac{-6 [12] [23] [13] [14] \langle 15 \rangle^2}{\langle 14 \rangle \langle 1|2+3|1|^3} \\
\tilde{r}_{15}^{+-} &= \frac{[14] [13] \langle 15 \rangle^2}{\langle 12 \rangle^2 \langle 34 \rangle \langle 1|2+5|1}} + & \tilde{r}_{32}^{+-} &= \frac{[12] \langle 12 \rangle [23] \langle 45 \rangle [14] \langle 15 \rangle}{\langle 14 \rangle^2 \langle 23 \rangle \langle 1|2+3|1} + \\
& & & \frac{-(12) [23] \langle 35 \rangle \langle 45 \rangle \langle 15 \rangle [15]}{\langle 14 \rangle^3 \langle 23 \rangle^2 \langle 1|2+3|1}} + \\
& & & \frac{2 [12] \langle 12 \rangle [23] \langle 45 \rangle \langle 15 \rangle}{\langle 14 \rangle^3 \langle 23 \rangle \langle 1|2+3|1}} + \\
& & & \frac{-\langle 35 \rangle [35] \langle 45 \rangle \langle 15 \rangle}{\langle 14 \rangle^3 \langle 23 \rangle^2} + \\
& & & \frac{\langle 25 \rangle \langle 45 \rangle [24]}{\langle 14 \rangle^2 \langle 23 \rangle^2} \\
& & & (12345 \rightarrow -21435) \\
\tilde{r}_{16}^{+-} &= \frac{\langle 35 \rangle \langle 45 \rangle [34]^2}{\langle 12 \rangle^2 \langle 34 \rangle \langle 3|1+2|3}} + & \tilde{r}_{33}^{+-} &= \frac{[24] [14] [13] \langle 15 \rangle}{\langle 14 \rangle \langle 23 \rangle [45] \langle 1|2+3|1}} + \\
& & & \frac{-\langle 25 \rangle [12] [24] [13]}{\langle 12 \rangle [15] \langle 34 \rangle \langle 2|1+5|2}} + \\
& & & \frac{2 [12] [14] [13] \langle 15 \rangle^2}{\langle 14 \rangle \langle 23 \rangle \langle 1|2+3|1} + \\
& & & \frac{-2 \langle 25 \rangle^2 [12] [24] [23]}{\langle 12 \rangle \langle 34 \rangle \langle 2|1+5|2} + \\
& & & (12345 \rightarrow -43215) + \\
& & & \frac{-\langle 24 \rangle [13] \langle 13 \rangle [14] [24]}{\langle 12 \rangle \langle 14 \rangle [15] \langle 23 \rangle \langle 34 \rangle [45]}
\end{aligned}$$

Appendix C: Five-gluon MHV basis functions

$$\begin{aligned}
\tilde{r}_1^{--} &= \frac{\langle 45 \rangle^2}{\langle 12 \rangle \langle 13 \rangle \langle 23 \rangle} & \tilde{r}_{20}^{--} &= \frac{[13]^2 \langle 45 \rangle}{\langle 23 \rangle \langle 25 \rangle [35] [45]} & \tilde{r}_{39}^{--} &= \frac{\langle 25 \rangle^3 [23]^2}{\langle 12 \rangle^2 \langle 23 \rangle [34]^2 \langle 35 \rangle} \\
\tilde{r}_2^{--} &= \frac{\langle 45 \rangle^3}{\langle 12 \rangle^2 \langle 34 \rangle \langle 35 \rangle} & \tilde{r}_{21}^{--} &= \frac{[23] \langle 45 \rangle^2}{\langle 12 \rangle \langle 13 \rangle \langle 35 \rangle [35]} & \tilde{r}_{40}^{--} &= \frac{\langle 25 \rangle^3 [25]^2}{\langle 12 \rangle^2 \langle 23 \rangle \langle 35 \rangle [45]^2} \\
\tilde{r}_3^{--} &= \frac{\langle 45 \rangle^3}{\langle 12 \rangle \langle 15 \rangle \langle 23 \rangle \langle 34 \rangle} & \tilde{r}_{22}^{--} &= \frac{[13] [23]^2}{\langle 12 \rangle [25] [34] [45]} & \tilde{r}_{41}^{--} &= \frac{[12] \langle 35 \rangle \langle 15 \rangle \langle 14 \rangle}{\langle 12 \rangle \langle 13 \rangle^3 [14]} \\
\tilde{r}_4^{--} &= \frac{[14] [12] [35]}{\langle 23 \rangle [45]^3} & \tilde{r}_{23}^{--} &= \frac{[12]^2 \langle 45 \rangle}{\langle 13 \rangle [15] \langle 23 \rangle [24]} & \tilde{r}_{42}^{--} &= \frac{\langle 45 \rangle^3 [23]}{\langle 14 \rangle \langle 15 \rangle \langle 23 \rangle \langle 24 \rangle [24]} \\
\tilde{r}_5^{--} &= \frac{\langle 45 \rangle^2 \langle 24 \rangle}{\langle 12 \rangle^2 \langle 23 \rangle \langle 34 \rangle} & \tilde{r}_{24}^{--} &= \frac{\langle 25 \rangle \langle 34 \rangle^2 [12]}{\langle 13 \rangle \langle 23 \rangle^3 [25]} & \tilde{r}_{43}^{--} &= \frac{[35] [15] \langle 35 \rangle \langle 25 \rangle}{\langle 12 \rangle \langle 23 \rangle^2 [45]^2} \\
\tilde{r}_6^{--} &= \frac{\langle 15 \rangle \langle 14 \rangle \langle 45 \rangle}{\langle 12 \rangle^2 \langle 13 \rangle^2} & \tilde{r}_{25}^{--} &= \frac{\langle 25 \rangle [14] [25]^2}{\langle 13 \rangle \langle 23 \rangle [45]^3} & \tilde{r}_{44}^{--} &= \frac{[25] \langle 25 \rangle^2 [13]}{\langle 12 \rangle^2 [14] \langle 23 \rangle [45]} \\
\tilde{r}_7^{--} &= \frac{[12]^2 \langle 45 \rangle}{\langle 34 \rangle \langle 35 \rangle [45]^2} & \tilde{r}_{26}^{--} &= \frac{[13] \langle 45 \rangle^3}{\langle 13 \rangle [14] \langle 15 \rangle \langle 24 \rangle^2} & \tilde{r}_{45}^{--} &= \frac{[12] \langle 45 \rangle^2 [13]}{\langle 12 \rangle \langle 14 \rangle [14]^2 \langle 34 \rangle} \\
\tilde{r}_8^{--} &= \frac{[25] [14]^2 [35]}{\langle 23 \rangle [45]^4} & \tilde{r}_{27}^{--} &= \frac{[13]^3 [25]}{\langle 12 \rangle [15]^2 [34] [45]} & \tilde{r}_{46}^{--} &= \frac{\langle 14 \rangle [34] \langle 45 \rangle^2}{\langle 12 \rangle^2 \langle 13 \rangle \langle 24 \rangle [24]} \\
\tilde{r}_9^{--} &= \frac{[23]^2 \langle 34 \rangle}{\langle 13 \rangle \langle 14 \rangle [45]^2} & \tilde{r}_{28}^{--} &= \frac{[12] \langle 45 \rangle^3}{\langle 14 \rangle \langle 24 \rangle \langle 35 \rangle^2 [45]} & \tilde{r}_{47}^{--} &= \frac{\langle 34 \rangle [13]^2 \langle 45 \rangle}{\langle 23 \rangle^2 [35] \langle 3 | 1+5 | 3]} \\
\tilde{r}_{10}^{--} &= \frac{[13]^2 \langle 34 \rangle \langle 24 \rangle}{\langle 23 \rangle^3 [35]^2} & \tilde{r}_{29}^{--} &= \frac{\langle 25 \rangle \langle 14 \rangle^2 \langle 24 \rangle \langle 45 \rangle}{\langle 12 \rangle^4 \langle 34 \rangle^2} & \tilde{r}_{48}^{--} &= \frac{[13] \langle 14 \rangle^2 \langle 15 \rangle [25]}{\langle 12 \rangle \langle 13 \rangle^3 [35]^2} \\
\tilde{r}_{11}^{--} &= \frac{\langle 34 \rangle \langle 14 \rangle \langle 45 \rangle^2}{\langle 13 \rangle^3 \langle 24 \rangle^2} & \tilde{r}_{30}^{--} &= \frac{[14] \langle 15 \rangle \langle 14 \rangle^2}{\langle 12 \rangle^2 \langle 13 \rangle^2 [45]} & \tilde{r}_{49}^{--} &= \frac{[12]^2 [23]^2 \langle 45 \rangle}{[24] [25] \langle 2 | 1+5 | 2 \rangle^2} \\
\tilde{r}_{12}^{--} &= \frac{\langle 34 \rangle \langle 14 \rangle \langle 35 \rangle^2}{\langle 13 \rangle^3 \langle 23 \rangle^2} & \tilde{r}_{31}^{--} &= \frac{\langle 34 \rangle [12]^2 \langle 24 \rangle}{\langle 13 \rangle^2 [15]^2 \langle 23 \rangle} & \tilde{r}_{50}^{--} &= \frac{\langle 24 \rangle^2 [12]^2 \langle 35 \rangle}{\langle 23 \rangle^3 [25] \langle 2 | 1+5 | 2 \rangle} \\
\tilde{r}_{13}^{--} &= \frac{\langle 35 \rangle^3 \langle 14 \rangle^2}{\langle 13 \rangle^4 \langle 23 \rangle \langle 25 \rangle} & \tilde{r}_{32}^{--} &= \frac{\langle 35 \rangle \langle 25 \rangle [23]^2}{\langle 12 \rangle^2 \langle 23 \rangle [24]^2} & \tilde{r}_{51}^{--} &= \frac{\langle 45 \rangle^2 [13]^2 \langle 14 \rangle}{\langle 13 \rangle \langle 25 \rangle^2 \langle 34 \rangle [35]^2} \\
\tilde{r}_{14}^{--} &= \frac{[12] [23] \langle 14 \rangle}{\langle 13 \rangle^2 [35] [45]} & \tilde{r}_{33}^{--} &= \frac{[13] \langle 34 \rangle \langle 35 \rangle^2}{\langle 13 \rangle^2 [14] \langle 23 \rangle^2} & \tilde{r}_{52}^{--} &= \frac{[12]^2 \langle 45 \rangle^2 \langle 23 \rangle}{\langle 12 \rangle \langle 13 \rangle [14]^2 \langle 34 \rangle^2} \\
\tilde{r}_{15}^{--} &= \frac{\langle 25 \rangle \langle 45 \rangle [13]}{\langle 12 \rangle^2 [14] \langle 23 \rangle} & \tilde{r}_{34}^{--} &= \frac{\langle 45 \rangle^2 [23]^2}{\langle 12 \rangle \langle 15 \rangle \langle 25 \rangle [25]^2} & \tilde{r}_{53}^{--} &= \frac{\langle 45 \rangle^2 \langle 15 \rangle [25]^2}{\langle 13 \rangle \langle 14 \rangle^2 \langle 35 \rangle [45]^2} \\
\tilde{r}_{16}^{--} &= \frac{[15] \langle 45 \rangle \langle 25 \rangle}{\langle 12 \rangle \langle 23 \rangle^2 [45]} & \tilde{r}_{35}^{--} &= \frac{[13]^2 \langle 45 \rangle^2}{\langle 13 \rangle [14] \langle 24 \rangle^2 [34]} & \tilde{r}_{54}^{--} &= \frac{[12]^2 \langle 35 \rangle [23]^3}{[24]^2 [25] \langle 2 | 1+5 | 2 \rangle^2} \\
\tilde{r}_{17}^{--} &= \frac{\langle 35 \rangle [13] \langle 24 \rangle}{\langle 12 \rangle \langle 23 \rangle^2 [45]} & \tilde{r}_{36}^{--} &= \frac{\langle 14 \rangle [13]^2 \langle 45 \rangle}{\langle 12 \rangle^2 \langle 15 \rangle [15]^2} & \tilde{r}_{55}^{--} &= \frac{\langle 34 \rangle [23] \langle 45 \rangle^2}{\langle 13 \rangle \langle 15 \rangle \langle 23 \rangle \langle 24 \rangle [25]} \\
\tilde{r}_{18}^{--} &= \frac{[12] \langle 24 \rangle \langle 45 \rangle}{\langle 12 \rangle \langle 23 \rangle^2 [25]} & \tilde{r}_{37}^{--} &= \frac{[34] \langle 34 \rangle^2 \langle 35 \rangle^2}{\langle 13 \rangle^3 \langle 23 \rangle^2 [14]} & \tilde{r}_{56}^{--} &= \frac{[23] [13] \langle 45 \rangle^2}{\langle 15 \rangle \langle 23 \rangle \langle 25 \rangle [25] [35]} \\
\tilde{r}_{19}^{--} &= \frac{[13]^2 [23]}{\langle 23 \rangle [34] [35] [45]} & \tilde{r}_{38}^{--} &= \frac{\langle 45 \rangle \langle 24 \rangle^2 \langle 35 \rangle \langle 14 \rangle^2}{\langle 12 \rangle^4 \langle 34 \rangle^3} & \tilde{r}_{57}^{--} &= \frac{\langle 25 \rangle [25] \langle 45 \rangle^2}{\langle 13 \rangle \langle 15 \rangle \langle 23 \rangle \langle 24 \rangle [45]}
\end{aligned}$$

$$\begin{aligned}
\tilde{r}_{58}^{--} &= \frac{[12]\langle 45 \rangle^2 [23]}{\langle 12 \rangle [24] \langle 34 \rangle \langle 2 | 1+5 | 2 \rangle} & \tilde{r}_{77}^{--} &= \frac{\langle 34 \rangle \langle 45 \rangle [35] \langle 35 \rangle^2}{\langle 13 \rangle^2 \langle 23 \rangle^2 \langle 3 | 1+2 | 3 \rangle} & \tilde{r}_{92}^{--} &= \frac{[23]^2 \langle 25 \rangle \langle 24 \rangle^2}{\langle 12 \rangle^2 \langle 23 \rangle \langle 35 \rangle [35]^2} + \\
\tilde{r}_{59}^{--} &= \frac{[12]^2 [13] \langle 45 \rangle}{\langle 13 \rangle [14] [15] \langle 1 | 2+3 | 1 \rangle} & \tilde{r}_{78}^{--} &= \frac{\langle 34 \rangle [12] [23]^3 \langle 25 \rangle^2}{\langle 12 \rangle [24] \langle 2 | 1+5 | 2 \rangle^3} & & \frac{2 \langle 14 \rangle [23] \langle 25 \rangle^2 \langle 24 \rangle}{\langle 12 \rangle^3 \langle 23 \rangle \langle 35 \rangle [35]} \\
\tilde{r}_{60}^{--} &= \frac{[34] [12] [35] \langle 45 \rangle}{\langle 12 \rangle [45]^2 \langle 5 | 1+2 | 5 \rangle} & \tilde{r}_{79}^{--} &= \frac{\langle 45 \rangle^2 \langle 34 \rangle^2 [34]^2}{\langle 12 \rangle \langle 13 \rangle \langle 23 \rangle \langle 35 \rangle^2 [35]^2} & \tilde{r}_{93}^{--} &= \frac{2 \langle 25 \rangle^3 [25] \langle 14 \rangle \langle 24 \rangle}{\langle 12 \rangle^3 \langle 23 \rangle^2 \langle 35 \rangle [35]} + \\
\tilde{r}_{61}^{--} &= \frac{[13] \langle 34 \rangle \langle 24 \rangle [12]^2}{[15] \langle 23 \rangle^3 [23] [25]} & \tilde{r}_{80}^{--} &= \frac{\langle 45 \rangle^2 \langle 35 \rangle^2 [35] \langle 25 \rangle}{\langle 15 \rangle^2 \langle 23 \rangle^3 \langle 5 | 1+4 | 5 \rangle} & & \frac{-\langle 25 \rangle^3 [25]^2 \langle 24 \rangle^2}{\langle 12 \rangle^2 \langle 23 \rangle^3 \langle 35 \rangle [35]^2} \\
\tilde{r}_{62}^{--} &= \frac{[23] \langle 45 \rangle \langle 35 \rangle \langle 34 \rangle}{\langle 13 \rangle^2 \langle 23 \rangle \langle 3 | 1+2 | 3 \rangle} & \tilde{r}_{81}^{--} &= \frac{[12] \langle 45 \rangle [34] \langle 34 \rangle}{\langle 13 \rangle \langle 23 \rangle \langle 35 \rangle [35] [45]} & \tilde{r}_{94}^{--} &= \frac{-[12] [23]^2 \langle 14 \rangle \langle 23 \rangle}{\langle 13 \rangle^3 [13] [35] [45]} + \\
\tilde{r}_{63}^{--} &= \frac{[12] \langle 25 \rangle [23]^2 \langle 35 \rangle}{\langle 12 \rangle \langle 23 \rangle \langle 24 \rangle [24]^3} & \tilde{r}_{82}^{--} &= \frac{[12] \langle 35 \rangle \langle 45 \rangle^3 [25]}{\langle 12 \rangle [24]^2 \langle 25 \rangle \langle 34 \rangle^3} & & \frac{[12]^2 \langle 15 \rangle [23] \langle 23 \rangle}{\langle 13 \rangle^3 [13] [14] [45]} \\
\tilde{r}_{64}^{--} &= \frac{\langle 24 \rangle [23] \langle 25 \rangle^2 \langle 15 \rangle}{\langle 12 \rangle^3 \langle 23 \rangle [34] \langle 35 \rangle} & \tilde{r}_{83}^{--} &= \frac{[12] [13] \langle 45 \rangle \langle 25 \rangle^2}{\langle 12 \rangle [14]^2 \langle 15 \rangle \langle 23 \rangle \langle 24 \rangle} & \tilde{r}_{95}^{--} &= \frac{2 [25] [15] \langle 45 \rangle^3 [34]^2}{\langle 12 \rangle [45] \langle 5 | 1+2 | 5 \rangle^3} + \\
\tilde{r}_{65}^{--} &= \frac{[35]^2 \langle 25 \rangle \langle 15 \rangle \langle 45 \rangle}{\langle 12 \rangle^3 [45] \langle 5 | 1+2 | 5 \rangle} & \tilde{r}_{84}^{--} &= \frac{\langle 25 \rangle^2 \langle 24 \rangle [23]^2 [12]}{\langle 12 \rangle \langle 23 \rangle [34] \langle 2 | 1+5 | 2 \rangle^2} & & \frac{3 [35] \langle 15 \rangle [12] [13] \langle 45 \rangle}{\langle 12 \rangle [45] \langle 5 | 1+2 | 5 \rangle^2} \\
\tilde{r}_{66}^{--} &= \frac{[35] [12] \langle 45 \rangle^2 [34]}{\langle 12 \rangle [45] \langle 5 | 1+2 | 5 \rangle^2} & \tilde{r}_{85}^{--} &= \frac{[23] \langle 45 \rangle^4 \langle 12 \rangle \langle 23 \rangle^2}{\langle 13 \rangle^3 \langle 24 \rangle^2 \langle 25 \rangle^2 \langle 2 | 1+3 | 2 \rangle} & \tilde{r}_{96}^{--} &= \frac{2 [34] [14] [35] [25] \langle 45 \rangle}{\langle 12 \rangle [45]^3 \langle 5 | 1+2 | 5 \rangle} + \\
\tilde{r}_{67}^{--} &= \frac{\langle 14 \rangle^2 [24] \langle 24 \rangle^2 [34]}{\langle 12 \rangle^4 [25] \langle 34 \rangle [45]} & \tilde{r}_{86}^{--} &= \frac{\langle 24 \rangle \langle 25 \rangle [13] [23] \langle 35 \rangle}{\langle 12 \rangle \langle 23 \rangle^2 [34] \langle 2 | 1+5 | 2 \rangle} & & \frac{[34]^2 [15] [25] \langle 45 \rangle^2}{\langle 12 \rangle [45]^2 \langle 5 | 1+2 | 5 \rangle^2} \\
\tilde{r}_{68}^{--} &= \frac{\langle 25 \rangle^3 \langle 24 \rangle \langle 13 \rangle [25]}{\langle 12 \rangle^3 \langle 23 \rangle^2 \langle 35 \rangle [45]} & \tilde{r}_{87}^{--} &= \frac{\langle 15 \rangle^2 [23] [25] \langle 35 \rangle^2}{\langle 13 \rangle^4 [24] \langle 25 \rangle [34]} + \\
& & & (12345 \rightarrow 12354) & \tilde{r}_{97}^{--} &= \frac{-\langle 34 \rangle^2 \langle 45 \rangle [34] [12]}{\langle 13 \rangle \langle 14 \rangle [15] \langle 23 \rangle \langle 35 \rangle [45]} + \\
\tilde{r}_{69}^{--} &= \frac{[35]^2 \langle 35 \rangle^3 [25]}{\langle 13 \rangle \langle 15 \rangle \langle 23 \rangle \langle 34 \rangle [45]^3} & \tilde{r}_{88}^{--} &= \frac{[15]^2 \langle 45 \rangle^2 \langle 15 \rangle [14]}{\langle 23 \rangle^2 [45] \langle 4 | 1+5 | 4 \rangle^2} + \\
\tilde{r}_{70}^{--} &= \frac{[35]^2 \langle 45 \rangle \langle 35 \rangle^2}{\langle 12 \rangle \langle 15 \rangle \langle 23 \rangle \langle 34 \rangle [45]^2} & & (12345 \rightarrow -32154) & & \frac{-[14] [15] [25] \langle 25 \rangle \langle 45 \rangle}{\langle 23 \rangle^2 [45]^2 \langle 5 | 1+4 | 5 \rangle} \\
\tilde{r}_{71}^{--} &= \frac{\langle 25 \rangle [13]^3 \langle 35 \rangle^2}{\langle 12 \rangle [14]^3 \langle 15 \rangle \langle 23 \rangle \langle 24 \rangle} & \tilde{r}_{89}^{--} &= \frac{\langle 14 \rangle^2 [13]^2 \langle 24 \rangle [14]}{\langle 12 \rangle^3 \langle 15 \rangle [15]^3} + \\
\tilde{r}_{72}^{--} &= \frac{\langle 45 \rangle^3 [14] \langle 34 \rangle [24]}{\langle 14 \rangle \langle 24 \rangle \langle 35 \rangle^3 [45]^2} & & \frac{\langle 14 \rangle [13]^3 \langle 34 \rangle}{\langle 12 \rangle^2 \langle 15 \rangle [15]^3} & \tilde{r}_{99}^{--} &= \frac{-[12] \langle 24 \rangle [34] \langle 45 \rangle}{\langle 12 \rangle \langle 23 \rangle \langle 25 \rangle [25] [45]} + \\
\tilde{r}_{73}^{--} &= \frac{[14]^2 [23] \langle 14 \rangle^2}{\langle 12 \rangle \langle 13 \rangle [45]^2 \langle 1 | 2+3 | 1 \rangle} & \tilde{r}_{90}^{--} &= \frac{-3 \langle 45 \rangle [12] [13]}{\langle 23 \rangle [45] \langle 4 | 1+5 | 4 \rangle} + \\
\tilde{r}_{74}^{--} &= \frac{[12] [23]^3 \langle 35 \rangle^2}{\langle 12 \rangle [24]^3 \langle 34 \rangle \langle 2 | 1+5 | 2 \rangle} & & \frac{[23] [12] \langle 45 \rangle^2}{\langle 12 \rangle [24] \langle 34 \rangle \langle 4 | 1+5 | 4 \rangle} & & \frac{[35] [12] \langle 45 \rangle^2 [34]}{\langle 12 \rangle \langle 25 \rangle [25] [45] \langle 5 | 1+2 | 5 \rangle} \\
\tilde{r}_{75}^{--} &= \frac{\langle 25 \rangle^2 [23]^2 \langle 24 \rangle}{\langle 12 \rangle^2 \langle 23 \rangle [34] \langle 2 | 1+5 | 2 \rangle} & \tilde{r}_{91}^{--} &= \frac{2 \langle 24 \rangle^2 [13] [23]^2}{\langle 12 \rangle \langle 23 \rangle \langle 35 \rangle [35]^3} + \\
\tilde{r}_{76}^{--} &= \frac{[12] \langle 15 \rangle \langle 14 \rangle^2 \langle 25 \rangle}{\langle 12 \rangle^2 \langle 13 \rangle^2 \langle 1 | 2+5 | 1 \rangle} & & \frac{\langle 24 \rangle [13] [23] \langle 45 \rangle}{\langle 12 \rangle \langle 23 \rangle \langle 35 \rangle [35]^2} & \tilde{r}_{100}^{--} &= \frac{[35] \langle 25 \rangle^2 \langle 15 \rangle [25] \langle 45 \rangle^2}{\langle 12 \rangle^3 \langle 35 \rangle \langle 5 | 1+2 | 5 \rangle^2} + \\
& & & & & \frac{-3 [35] \langle 25 \rangle^2 \langle 15 \rangle \langle 14 \rangle \langle 45 \rangle}{\langle 12 \rangle^4 \langle 35 \rangle \langle 5 | 1+2 | 5 \rangle} \\
& & & & \tilde{r}_{101}^{--} &= \frac{[34] \langle 34 \rangle \langle 45 \rangle^2 [15] [14]}{\langle 23 \rangle^2 [45] \langle 4 | 1+5 | 4 \rangle^2} + \\
& & & & & \frac{-\langle 24 \rangle [23] \langle 34 \rangle \langle 45 \rangle [14]^2}{\langle 23 \rangle^2 [45] \langle 4 | 1+5 | 4 \rangle^2} + \\
& & & & & (12345 \rightarrow -32154)
\end{aligned}$$

$$\begin{aligned}
\tilde{r}_{102}^- &= \frac{-2\langle 14 \rangle [25] \langle 35 \rangle^2 \langle 34 \rangle}{\langle 13 \rangle^4 [15] \langle 23 \rangle} + \\
&\quad \frac{\langle 34 \rangle \langle 24 \rangle \langle 35 \rangle^2 [25]^2}{\langle 13 \rangle^4 [15]^2 \langle 23 \rangle} + \\
&\quad \frac{-2[12] \langle 35 \rangle \langle 34 \rangle^2 [35]}{\langle 13 \rangle^3 [15]^2 \langle 23 \rangle} \\
\tilde{r}_{103}^- &= \frac{3\langle 45 \rangle \langle 35 \rangle^2 [25]^2 \langle 15 \rangle^2}{\langle 13 \rangle^4 [24] \langle 25 \rangle \langle 5 | 1+3 | 5]} + \\
&\quad \frac{3[23] \langle 35 \rangle^2 [25] \langle 15 \rangle^2}{\langle 13 \rangle^4 [24] \langle 25 \rangle [34]} + \\
&\quad \frac{-(34)^2 \langle 45 \rangle [24]}{\langle 13 \rangle^3 [15] \langle 23 \rangle} \\
\tilde{r}_{104}^- &= \frac{2\langle 24 \rangle^2 \langle 34 \rangle^2 \langle 5 | 3-4 | 2 \rangle}{\langle 14 \rangle^2 \langle 23 \rangle^4 [25]} + \\
&\quad \frac{-(12)[12]^2 \langle 34 \rangle^2 \langle 24 \rangle}{\langle 14 \rangle \langle 23 \rangle^4 [25]^2} + \\
&\quad \frac{-2[12] \langle 24 \rangle \langle 34 \rangle^2 [23]}{\langle 14 \rangle \langle 23 \rangle^3 [25]^2} \\
\tilde{r}_{105}^- &= \frac{-2\langle 12 \rangle [12]^3 [13]}{\langle 13 \rangle [14] [15] [45] \langle 1 | 2+3 | 1 \rangle} + \\
&\quad \frac{-[12] \langle 24 \rangle [34] \langle 34 \rangle^2}{\langle 13 \rangle \langle 14 \rangle [15] \langle 23 \rangle^2 [45]} + \\
&\quad \frac{[35] [13] \langle 35 \rangle^3}{\langle 13 \rangle [14] \langle 15 \rangle \langle 23 \rangle^2 [45]} \\
\tilde{r}_{106}^- &= \frac{2\langle 15 \rangle \langle 45 \rangle [13] [23]}{\langle 12 \rangle \langle 14 \rangle [34] \langle 35 \rangle [45]} + \\
&\quad \frac{2\langle 25 \rangle \langle 45 \rangle [24] [13]}{\langle 12 \rangle \langle 23 \rangle \langle 35 \rangle [34] [45]} + \\
&\quad \frac{-[35] \langle 25 \rangle \langle 45 \rangle^2 [23]}{\langle 12 \rangle \langle 14 \rangle \langle 24 \rangle [34] \langle 35 \rangle [45]} \\
\tilde{r}_{107}^- &= \frac{-[25] \langle 25 \rangle \langle 15 \rangle^2 \langle 14 \rangle [13]}{\langle 12 \rangle^2 \langle 13 \rangle^2 \langle 34 \rangle [34]^2} + \\
&\quad \frac{-[24] \langle 14 \rangle^2 \langle 24 \rangle [13]}{\langle 12 \rangle^2 \langle 13 \rangle \langle 34 \rangle [35] [45]} + \\
&\quad \frac{2[13] \langle 14 \rangle^2 \langle 25 \rangle [23]}{\langle 12 \rangle^2 \langle 13 \rangle \langle 34 \rangle [34] [35]} \\
\tilde{r}_{108}^- &= \frac{\langle 45 \rangle^3 [13]^2 \langle 13 \rangle^2}{\langle 12 \rangle^2 \langle 34 \rangle \langle 35 \rangle \langle 3 | 1+2 | 3 \rangle^2} + \\
&\quad \frac{-\langle 24 \rangle \langle 13 \rangle^2 [13] \langle 45 \rangle^3}{\langle 12 \rangle^3 \langle 34 \rangle^2 \langle 35 \rangle \langle 3 | 1+2 | 3 \rangle} + \\
&\quad \frac{-\langle 45 \rangle^3 [13] \langle 25 \rangle \langle 13 \rangle^2}{\langle 12 \rangle^3 \langle 34 \rangle \langle 35 \rangle^2 \langle 3 | 1+2 | 3 \rangle} \\
\tilde{r}_{109}^- &= \frac{-(34) \langle 35 \rangle [13] [23] \langle 45 \rangle}{\langle 13 \rangle \langle 23 \rangle \langle 3 | 1+2 | 3 \rangle^2} + \\
&\quad \frac{-2\langle 34 \rangle [23]^2 \langle 35 \rangle^2 \langle 24 \rangle}{\langle 13 \rangle^2 \langle 23 \rangle \langle 3 | 1+2 | 3 \rangle^2} + \\
&\quad \frac{2\langle 34 \rangle [23] \langle 35 \rangle^2 \langle 24 \rangle}{\langle 13 \rangle^2 \langle 23 \rangle^2 \langle 3 | 1+2 | 3 \rangle} + \\
&\quad (12345 \rightarrow -21354) \\
\tilde{r}_{110}^- &= \frac{-2\langle 25 \rangle \langle 45 \rangle [25] [13] \langle 35 \rangle}{\langle 13 \rangle [14] \langle 15 \rangle \langle 23 \rangle \langle 24 \rangle [45]} + \\
&\quad \frac{[12] \langle 45 \rangle [23] [34]}{\langle 15 \rangle [45]^2 \langle 4 | 1+2 | 4 \rangle} + \\
&\quad \frac{[35] \langle 23 \rangle \langle 45 \rangle^2 [24]^2 [13]}{\langle 13 \rangle [14] \langle 15 \rangle \langle 24 \rangle [45]^2 \langle 4 | 1+2 | 4 \rangle} \\
\tilde{r}_{111}^- &= \frac{[35] \langle 15 \rangle \langle 45 \rangle \langle 35 \rangle}{\langle 12 \rangle^2 \langle 13 \rangle \langle 23 \rangle [24]} + \\
&\quad \frac{\langle 25 \rangle \langle 15 \rangle \langle 14 \rangle [45] \langle 45 \rangle}{\langle 12 \rangle^3 \langle 13 \rangle \langle 23 \rangle [24]} + \\
&\quad \frac{-3[35] \langle 25 \rangle \langle 15 \rangle \langle 14 \rangle \langle 35 \rangle}{\langle 12 \rangle^3 \langle 13 \rangle \langle 23 \rangle [24]} + \\
&\quad \frac{-3[35] \langle 25 \rangle^2 \langle 14 \rangle [34] \langle 35 \rangle}{\langle 12 \rangle^4 [14] \langle 23 \rangle [24]} \\
\tilde{r}_{112}^- &= \frac{-3\langle 14 \rangle [12]^2 \langle 15 \rangle^2 [13]^2 \langle 34 \rangle}{\langle 13 \rangle \langle 1 | 2+5 | 1 \rangle^4} + \\
&\quad \frac{2\langle 14 \rangle [12] \langle 15 \rangle^2 [13] [15] \langle 45 \rangle}{\langle 12 \rangle \langle 13 \rangle \langle 1 | 2+5 | 1 \rangle^3} + \\
&\quad \frac{-2\langle 14 \rangle [12]^2 \langle 15 \rangle^2 [13] \langle 34 \rangle}{\langle 13 \rangle^2 \langle 1 | 2+5 | 1 \rangle^3} + \\
&\quad \frac{-[12]^2 \langle 15 \rangle \langle 14 \rangle^2 \langle 35 \rangle}{\langle 13 \rangle^3 \langle 1 | 2+5 | 1 \rangle^2} \\
\tilde{r}_{113}^- &= \frac{2[35] \langle 34 \rangle \langle 5 | 1+2 | 5 \rangle \langle 14 \rangle^2 [34] \langle 15 \rangle}{\langle 12 \rangle^4 \langle 13 \rangle \langle 25 \rangle [25]^3} + \\
&\quad \frac{2\langle 34 \rangle \langle 5 | 1+2 | 5 \rangle \langle 14 \rangle^2 [34] [23]}{\langle 12 \rangle^3 \langle 13 \rangle \langle 25 \rangle [25]^3} + \\
&\quad \frac{2\langle 34 \rangle \langle 14 \rangle^2 [34] [12] [23]}{\langle 12 \rangle^2 \langle 13 \rangle \langle 25 \rangle [25]^3} + \\
&\quad \frac{\langle 45 \rangle \langle 14 \rangle^2 \langle 34 \rangle [34]^2}{\langle 12 \rangle^3 \langle 13 \rangle \langle 25 \rangle [25]^2} \\
\tilde{r}_{114}^- &= \frac{[12]^2 [23]^2}{\langle 13 \rangle [15] [24]^2 [35]} + \\
&\quad \frac{\langle 45 \rangle^3 \langle 2 | 1+5 | 2 \rangle}{\langle 13 \rangle \langle 15 \rangle \langle 23 \rangle \langle 24 \rangle^2 [24]} + \\
&\quad \frac{-[12] \langle 45 \rangle^2 \langle 25 \rangle [25]}{\langle 13 \rangle \langle 23 \rangle \langle 24 \rangle^2 [24]^2} + \\
&\quad \frac{[23]^2 \langle 45 \rangle^2 \langle 5 | 1+3 | 5 \rangle}{\langle 13 \rangle \langle 15 \rangle \langle 24 \rangle^2 [24]^2 [35]} + \\
&\quad \frac{-[12] [23]^2 [13] \langle 34 \rangle}{\langle 13 \rangle [15] [24] [35] \langle 3 | 1+5 | 3 \rangle} + \\
&\quad \frac{-2[12]^2 [23]^2 [13]}{[15] [24]^2 [35] \langle 3 | 1+5 | 3 \rangle} + \\
&\quad \frac{-[23]^2 [13] \langle 45 \rangle^2 [15]}{\langle 24 \rangle^2 [24]^2 [35] \langle 3 | 1+5 | 3 \rangle} + \\
&\quad \frac{-2[23]^3 \langle 34 \rangle \langle 35 \rangle}{\langle 13 \rangle^2 [24] [35] \langle 3 | 1+5 | 3 \rangle} + \\
&\quad \frac{[23]^2 \langle 35 \rangle \langle 34 \rangle \langle 14 \rangle [13]^2}{\langle 13 \rangle \langle 24 \rangle [24] [35] \langle 3 | 1+5 | 3 \rangle^2} + \\
&\quad \frac{3[12] [23]^3 [13] \langle 35 \rangle}{[24]^2 [35] \langle 3 | 1+5 | 3 \rangle^2} + \\
&\quad \frac{3[23]^3 [13]^2 \langle 34 \rangle \langle 35 \rangle}{[24] [35] \langle 3 | 1+5 | 3 \rangle^3} + \\
&\quad \frac{-3[23]^3 [13] \langle 34 \rangle \langle 35 \rangle^2}{\langle 13 \rangle [24] \langle 3 | 1+5 | 3 \rangle^3} \\
\tilde{r}_{115}^- &= \frac{-2/3 [24]^2 \langle 24 \rangle \langle 45 \rangle \langle 14 \rangle^2}{\langle 12 \rangle \langle 13 \rangle^3 \langle 35 \rangle [35]^2} + \\
&\quad \frac{2/3 \langle 24 \rangle^2 [23] [24]^2 [25] \langle 14 \rangle}{\langle 13 \rangle^3 \langle 35 \rangle [35]^3 [45]} + \\
&\quad \frac{-[23]^3 [13] \langle 5 | 1+3 | 5 \rangle}{\langle 13 \rangle [24] [34] \langle 35 \rangle [35]^3} + \\
&\quad \frac{5/3 \langle 24 \rangle [23] [24] \langle 14 \rangle^2 [13]}{\langle 12 \rangle \langle 13 \rangle^2 \langle 35 \rangle [35]^3} + \\
&\quad \frac{-5/6 [23] \langle 2 | 1+3 | 2 \rangle \langle 45 \rangle \langle 14 \rangle}{\langle 12 \rangle \langle 13 \rangle^2 \langle 35 \rangle [35]^2} + \\
&\quad \frac{2/3 [23] [13] \langle 14 \rangle \langle 2 | 5-4 | 2 \rangle}{\langle 12 \rangle \langle 13 \rangle \langle 35 \rangle [35]^2 [45]} + \\
&\quad \frac{1/6 \langle 25 \rangle^2 [23] [25]^2 \langle 14 \rangle}{\langle 12 \rangle \langle 13 \rangle^2 \langle 35 \rangle [35]^2 [45]} + \\
&\quad \frac{[23] \langle 25 \rangle [25] \langle 14 \rangle \langle 45 \rangle}{\langle 12 \rangle \langle 13 \rangle^2 \langle 35 \rangle [35]^2} + \\
&\quad \frac{-1/2 \langle 25 \rangle \langle 45 \rangle [25]^2 \langle 15 \rangle}{\langle 12 \rangle \langle 13 \rangle^2 \langle 35 \rangle [35] [45]} + \\
&\quad \frac{-1/2 \langle 25 \rangle [23]^2 \langle 5 | 1+3 | 5 \rangle}{\langle 12 \rangle \langle 13 \rangle [34] \langle 35 \rangle [35] [45]}
\end{aligned}$$

Appendix D: Reference evaluations

To facilitate comparison with our results, we provide a numerical evaluation of the hard function defined in eqs. (21) and (22). We evaluate B and $H^{(L),(n_c,n_f)}$ on the phase-space point

$$\begin{aligned}
 p_1 &= \{-3.6033749869055013, 3.5549594933215615, 0.033937560795432568, 0.58772658529828721\}, \\
 p_2 &= \{-3.5779991067160259, 3.5333697062718894, 0.033731453043168395, -0.56235070510881185\}, \\
 p_3 &= \{1.7967619455543639, -1.7454551820128482, 0.10779867188908804, -0.41245501926361226\}, \\
 p_4 &= \{0.41554983516150722, -0.38259279840807596, -0.13137170294301400, 0.095109893149375643\}, \\
 p_5 &= \{4.9690623129056561, -4.9602812191725268, -0.044095982784675001, 0.29196924592476125\},
 \end{aligned} \tag{D1}$$

and the renormalization scale is set to $\mu = 1$.

The reference evaluations are

$$\begin{aligned}
 B &= 154023.6666921499, & H^{(2),(2,0)} &= 39.18504944322860, \\
 & & H^{(2),(0,0)} &= 181.8421831216970, \\
 H^{(1),(1,0)} &= -1.616272307398762, & H^{(2),(1,1)} &= -3.524523895322017, \\
 H^{(1),(-1,0)} &= 1.410723596231933, & H^{(2),(-1,1)} &= -6.578862105257153, \\
 & & H^{(2),(-3,1)} &= 0.01653881075908589, \\
 H^{(1),(0,1)} &= 2.508992268209689, & H^{(2),(0,2)} &= 1.703372292225135, \\
 H^{(1),(-2,1)} &= -0.04224997482253675, & H^{(2),(-2,2)} &= -0.4017699546907486, \\
 & & H^{(2),(-4,2)} &= 1.039350843363634.
 \end{aligned} \tag{D2}$$

-
- [1] M. Czakon, A. Mitov, and R. Poncelet, Next-to-Next-to-Leading Order Study of Three-Jet Production at the LHC, *Phys. Rev. Lett.* **127**, 152001 (2021), [Erratum: *Phys.Rev.Lett.* 129, 119901 (2022), Erratum: *Phys.Rev.Lett.* 129, 119901 (2022)], arXiv:2106.05331 [hep-ph].
- [2] G. Aad *et al.* (ATLAS), Determination of the strong coupling constant from transverse energy–energy correlations in multijet events at $\sqrt{s} = 13$ TeV with the ATLAS detector, *JHEP* **07**, 085, arXiv:2301.09351 [hep-ex].
- [3] M. Alvarez, J. Cantero, M. Czakon, J. Llorente, A. Mitov, and R. Poncelet, NNLO QCD corrections to event shapes at the LHC, *JHEP* **03**, 129, arXiv:2301.01086 [hep-ph].
- [4] X. Chen, T. Gehrmann, E. W. N. Glover, A. Huss, and M. Marcoli, Automation of antenna subtraction in colour space: gluonic processes, *JHEP* **10**, 099, arXiv:2203.13531 [hep-ph].
- [5] S. Abreu, F. Febres Cordero, H. Ita, B. Page, and V. Sotnikov, Leading-color two-loop QCD corrections for three-jet production at hadron colliders, *JHEP* **07**, 095, arXiv:2102.13609 [hep-ph].
- [6] X. Chen, T. Gehrmann, E. W. N. Glover, A. Huss, and J. Mo, NNLO QCD corrections in full colour for jet production observables at the LHC, *JHEP* **09**, 025, arXiv:2204.10173 [hep-ph].
- [7] S. Catani, D. de Florian, and G. Rodrigo, Space-like (versus time-like) collinear limits in QCD: Is factorization violated?, *JHEP* **07**, 026, arXiv:1112.4405 [hep-ph].
- [8] J. R. Forshaw, M. H. Seymour, and A. Siodmok, On the Breaking of Collinear Factorization in QCD, *JHEP* **11**, 066, arXiv:1206.6363 [hep-ph].
- [9] L. J. Dixon, E. Herrmann, K. Yan, and H. X. Zhu, Soft gluon emission at two loops in full color, *JHEP* **05**, 135, arXiv:1912.09370 [hep-ph].
- [10] G. De Laurentis, H. Ita, and V. Sotnikov, Double-Virtual NNLO QCD Corrections for Five-Parton Scattering: The Quark Channels, (2023), arXiv:2311.18752 [hep-ph].
- [11] C. G. Papadopoulos, D. Tommasini, and C. Wever, The Pentabox Master Integrals with the Simplified Differential Equations approach, *JHEP* **04**, 078, arXiv:1511.09404 [hep-ph].
- [12] T. Gehrmann, J. M. Henn, and N. A. Lo Presti, Pentagon functions for massless planar scattering amplitudes, *JHEP* **10**, 103, arXiv:1807.09812 [hep-ph].
- [13] S. Abreu, L. J. Dixon, E. Herrmann, B. Page, and M. Zeng, The two-loop five-point amplitude in $\mathcal{N} = 4$ super-Yang-Mills theory, *Phys. Rev. Lett.* **122**, 121603 (2019), arXiv:1812.08941 [hep-th].
- [14] D. Chicherin, T. Gehrmann, J. M. Henn, P. Wasser, Y. Zhang, and S. Zoia, All Master Integrals for Three-Jet Production at Next-to-Next-to-Leading Order, *Phys. Rev. Lett.* **123**, 041603 (2019), arXiv:1812.11160 [hep-ph].
- [15] D. Chicherin and V. Sotnikov, Pentagon Functions for Scattering of Five Massless Particles, *JHEP* **20**, 167, arXiv:2009.07803 [hep-ph].
- [16] A. von Manteuffel and R. M. Schabinger, A novel

- approach to integration by parts reduction, *Phys. Lett. B* **744**, 101 (2015), [arXiv:1406.4513 \[hep-ph\]](#).
- [17] T. Peraro, Scattering amplitudes over finite fields and multivariate functional reconstruction, *JHEP* **12**, 030, [arXiv:1608.01902 \[hep-ph\]](#).
- [18] J. Klappert, F. Lange, P. Maierhöfer, and J. Usövitsch, Integral reduction with Kira 2.0 and finite field methods, *Comput. Phys. Commun.* **266**, 108024 (2021), [arXiv:2008.06494 \[hep-ph\]](#).
- [19] V. Magerya, Rational Tracer: a Tool for Faster Rational Function Reconstruction, (2022), [arXiv:2211.03572 \[physics.data-an\]](#).
- [20] A. V. Belitsky, A. V. Smirnov, and R. V. Yakovlev, Balancing act: Multivariate rational reconstruction for IBP, *Nucl. Phys. B* **993**, 116253 (2023), [arXiv:2303.02511 \[hep-ph\]](#).
- [21] G. De Laurentis and B. Page, Ansätze for scattering amplitudes from p-adic numbers and algebraic geometry, *JHEP* **12**, 140, [arXiv:2203.04269 \[hep-th\]](#).
- [22] S. Badger, C. Brønnum-Hansen, D. Chicherin, T. Gehrmann, H. B. Hartanto, J. Henn, M. Marcoli, R. Moodie, T. Peraro, and S. Zoia, Virtual QCD corrections to gluon-initiated diphoton plus jet production at hadron colliders, *JHEP* **11**, 083, [arXiv:2106.08664 \[hep-ph\]](#).
- [23] S. Abreu, F. Febres Cordero, H. Ita, M. Klinkert, B. Page, and V. Sotnikov, Leading-color two-loop amplitudes for four partons and a W boson in QCD, *JHEP* **04**, 042, [arXiv:2110.07541 \[hep-ph\]](#).
- [24] S. Abreu, J. Dormans, F. Febres Cordero, H. Ita, and B. Page, Analytic Form of Planar Two-Loop Five-Gluon Scattering Amplitudes in QCD, *Phys. Rev. Lett.* **122**, 082002 (2019), [arXiv:1812.04586 \[hep-ph\]](#).
- [25] X. Liu, Reconstruction of rational functions made simple, (2023), [arXiv:2306.12262 \[hep-ph\]](#).
- [26] G. De Laurentis and D. Maître, Extracting analytical one-loop amplitudes from numerical evaluations, *JHEP* **07**, 123, [arXiv:1904.04067 \[hep-ph\]](#).
- [27] G. De Laurentis and D. Maître, Two-Loop Five-Parton Leading-Colour Finite Remainders in the Spinor-Helicity Formalism, *JHEP* **02**, 016, [arXiv:2010.14525 \[hep-ph\]](#).
- [28] J. M. Campbell, G. De Laurentis, and R. K. Ellis, Vector boson pair production at one loop: analytic results for the process $q\bar{q}\ell\bar{\ell}\ell'\bar{\ell}'g$, *JHEP* **07**, 096, [arXiv:2203.17170 \[hep-ph\]](#).
- [29] B. Agarwal, F. Buccioni, A. von Manteuffel, and L. Tancredi, Two-Loop Helicity Amplitudes for Diphoton Plus Jet Production in Full Color, *Phys. Rev. Lett.* **127**, 262001 (2021), [arXiv:2105.04585 \[hep-ph\]](#).
- [30] S. Badger, M. Czakon, H. B. Hartanto, R. Moodie, T. Peraro, R. Poncelet, and S. Zoia, Isolated photon production in association with a jet pair through next-to-next-to-leading order in QCD, *JHEP* **10**, 071, [arXiv:2304.06682 \[hep-ph\]](#).
- [31] H. Ita, Two-loop Integrand Decomposition into Master Integrals and Surface Terms, *Phys. Rev. D* **94**, 116015 (2016), [arXiv:1510.05626 \[hep-th\]](#).
- [32] S. Abreu, F. Febres Cordero, H. Ita, M. Jaquier, B. Page, and M. Zeng, Two-Loop Four-Gluon Amplitudes from Numerical Unitarity, *Phys. Rev. Lett.* **119**, 142001 (2017), [arXiv:1703.05273 \[hep-ph\]](#).
- [33] S. Abreu, F. Febres Cordero, H. Ita, B. Page, and M. Zeng, Planar Two-Loop Five-Gluon Amplitudes from Numerical Unitarity, *Phys. Rev. D* **97**, 116014 (2018), [arXiv:1712.03946 \[hep-ph\]](#).
- [34] S. Abreu, J. Dormans, F. Febres Cordero, H. Ita, M. Kraus, B. Page, E. Pascual, M. S. Ruf, and V. Sotnikov, Caravel: A C++ framework for the computation of multi-loop amplitudes with numerical unitarity, *Comput. Phys. Commun.* **267**, 108069 (2021), [arXiv:2009.11957 \[hep-ph\]](#).
- [35] S. Abreu, G. De Laurentis, H. Ita, M. Klinkert, B. Page, and V. Sotnikov, Two-Loop QCD Corrections for Three-Photon Production at Hadron Colliders, *SciPost Phys.* **15**, 157 (2023), [arXiv:2305.17056 \[hep-ph\]](#).
- [36] G. De Laurentis, H. Ita, B. Page, and V. Sotnikov, in preparation (2024).
- [37] S. Badger, D. Chicherin, T. Gehrmann, G. Heinrich, J. M. Henn, T. Peraro, P. Wasser, Y. Zhang, and S. Zoia, Analytic form of the full two-loop five-gluon all-plus helicity amplitude, *Phys. Rev. Lett.* **123**, 071601 (2019), [arXiv:1905.03733 \[hep-ph\]](#).
- [38] D. C. Dunbar, J. H. Godwin, W. B. Perkins, and J. M. W. Strong, Color Dressed Unitarity and Recursion for Yang-Mills Two-Loop All-Plus Amplitudes, *Phys. Rev. D* **101**, 016009 (2020), [arXiv:1911.06547 \[hep-ph\]](#).
- [39] D. A. Kosower and S. Pögel, A Unitarity Approach to Two-Loop All-Plus Rational Terms, (2022), [arXiv:2206.14445 \[hep-ph\]](#).
- [40] B. Agarwal, F. Buccioni, F. Devoto, G. Gambuti, A. von Manteuffel, and L. Tancredi, Five-Parton Scattering in QCD at Two Loops, (2023), [arXiv:2311.09870 \[hep-ph\]](#).
- [41] D. Maître and P. Mastrolia, S@M, a Mathematica Implementation of the Spinor-Helicity Formalism, *Comput. Phys. Commun.* **179**, 501 (2008), [arXiv:0710.5559 \[hep-ph\]](#).
- [42] Z. Bern and D. A. Kosower, Color decomposition of one loop amplitudes in gauge theories, *Nucl. Phys. B* **362**, 389 (1991).
- [43] G. 't Hooft, A Planar Diagram Theory for Strong Interactions, *Nucl. Phys. B* **72**, 461 (1974).
- [44] Z. Bern, L. J. Dixon, and D. A. Kosower, One loop corrections to five gluon amplitudes, *Phys. Rev. Lett.* **70**, 2677 (1993), [arXiv:hep-ph/9302280](#).
- [45] S. Badger, G. Mogull, A. Ochirov, and D. O'Connell, A Complete Two-Loop, Five-Gluon Helicity Amplitude in Yang-Mills Theory, *JHEP* **10**, 064, [arXiv:1507.08797 \[hep-ph\]](#).
- [46] S. Badger, C. Brønnum-Hansen, H. B. Hartanto, and T. Peraro, Analytic helicity amplitudes for two-loop five-gluon scattering: the single-minus case, *JHEP* **01**, 186, [arXiv:1811.11699 \[hep-ph\]](#).
- [47] S. Abreu, J. Dormans, F. Febres Cordero, H. Ita, B. Page, and V. Sotnikov, Analytic Form of the Planar Two-Loop Five-Parton Scattering Amplitudes in QCD, *JHEP* **05**, 084, [arXiv:1904.00945 \[hep-ph\]](#).

- [48] S. Catani, The Singular behavior of QCD amplitudes at two loop order, *Phys. Lett. B* **427**, 161 (1998), [arXiv:hep-ph/9802439](#).
- [49] G. F. Sterman and M. E. Tejeda-Yeomans, Multi-loop amplitudes and resummation, *Phys. Lett. B* **552**, 48 (2003), [arXiv:hep-ph/0210130](#).
- [50] T. Becher and M. Neubert, Infrared singularities of scattering amplitudes in perturbative QCD, *Phys. Rev. Lett.* **102**, 162001 (2009), [Erratum: *Phys.Rev.Lett.* 111, 199905 (2013)], [arXiv:0901.0722 \[hep-ph\]](#).
- [51] E. Gardi and L. Magnea, Factorization constraints for soft anomalous dimensions in QCD scattering amplitudes, *JHEP* **03**, 079, [arXiv:0901.1091 \[hep-ph\]](#).
- [52] T. Becher and M. Neubert, On the Structure of Infrared Singularities of Gauge-Theory Amplitudes, *JHEP* **06**, 081, [Erratum: *JHEP* 11, 024 (2013)], [arXiv:0903.1126 \[hep-ph\]](#).
- [53] S. Weinzierl, Does one need the $O(\epsilon)$ - and $O(\epsilon^2)$ -terms of one-loop amplitudes in an NNLO calculation ?, *Phys. Rev. D* **84**, 074007 (2011), [arXiv:1107.5131 \[hep-ph\]](#).
- [54] A. C. Edison and S. G. Naculich, SU(N) group-theory constraints on color-ordered five-point amplitudes at all loop orders, *Nucl. Phys. B* **858**, 488 (2012), [arXiv:1111.3821 \[hep-th\]](#).
- [55] D. C. Dunbar, Identities amongst the two loop partial amplitudes of Yang-Mills theory, *JHEP* **10**, 058, [arXiv:2308.06602 \[hep-th\]](#).
- [56] P. Nogueira, Automatic Feynman graph generation, *J. Comput. Phys.* **105**, 279 (1993).
- [57] A. Ochirov and B. Page, Full Colour for Loop Amplitudes in Yang-Mills Theory, *JHEP* **02**, 100, [arXiv:1612.04366 \[hep-ph\]](#).
- [58] A. Ochirov and B. Page, Multi-Quark Colour Decompositions from Unitarity, *JHEP* **10**, 058, [arXiv:1908.02695 \[hep-ph\]](#).
- [59] S. Badger, C. Brønnum-Hansen, H. B. Hartanto, and T. Peraro, First look at two-loop five-gluon scattering in QCD, *Phys. Rev. Lett.* **120**, 092001 (2018), [arXiv:1712.02229 \[hep-ph\]](#).
- [60] S. Abreu, F. Febres Cordero, H. Ita, B. Page, and V. Sotnikov, Planar Two-Loop Five-Parton Amplitudes from Numerical Unitarity, *JHEP* **11**, 116, [arXiv:1809.09067 \[hep-ph\]](#).
- [61] B. Page, Sagex mathematica and maple schools: Lectures on finite fields and large ansätze (2021), <https://indico.desy.de/event/28075/>.
- [62] S. Abreu, B. Page, and M. Zeng, Differential equations from unitarity cuts: nonplanar hexa-box integrals, *JHEP* **01**, 006, [arXiv:1807.11522 \[hep-th\]](#).
- [63] S. Badger, H. B. Hartanto, and S. Zoia, Two-Loop QCD Corrections to Wbb^- Production at Hadron Colliders, *Phys. Rev. Lett.* **127**, 012001 (2021), [arXiv:2102.02516 \[hep-ph\]](#).
- [64] W. Decker, G.-M. Greuel, G. Pfister, and H. Schönemann, SINGULAR 4-3-0 — A computer algebra system for polynomial computations, <http://www.singular.uni-kl.de> (2022).
- [65] L. Perron and V. Furnon, OR-Tools, <https://developers.google.com/optimization/> (2023), Google.
- [66] G. De Laurentis, Lips: p -adic and singular phase space, in *21th International Workshop on Advanced Computing and Analysis Techniques in Physics Research: AI meets Reality* (2023) [arXiv:2305.14075 \[hep-th\]](#).
- [67] G. De Laurentis, H. Ita, M. Klinkert, and V. Sotnikov, Supplementary material for “Double-Virtual NNLO QCD Corrections for Five-Parton Scattering: The Gluon Channel” (2023).
- [68] C. F. Berger, Z. Bern, L. J. Dixon, F. Febres Cordero, D. Forde, H. Ita, D. A. Kosower, and D. Maitre, An Automated Implementation of On-Shell Methods for One-Loop Amplitudes, *Phys. Rev. D* **78**, 036003 (2008), [arXiv:0803.4180 \[hep-ph\]](#).
- [69] B. Agarwal, F. Buccioni, F. Devoto, G. Gambuti, A. von Manteuffel, and L. Tancredi, private correspondence (2023).
- [70] <https://gitlab.com/five-point-amplitudes/FivePointAmplitudes-cpp.git>.
- [71] D. Chicherin, V. Sotnikov, and S. Zoia, Pentagon functions for one-mass planar scattering amplitudes, *JHEP* **01**, 096, [arXiv:2110.10111 \[hep-ph\]](#).
- [72] S. Abreu, D. Chicherin, H. Ita, B. Page, V. Sotnikov, W. Tschernow, and S. Zoia, All Two-Loop Feynman Integrals for Five-Point One-Mass Scattering, (2023), [arXiv:2306.15431 \[hep-ph\]](#).